ABSTRACT

HOBAN, NICOLE PRENTICE. Observed Characteristics of Mesoscale Banding in Coastal Northeast U.S. Snow Storms. (Under the direction of Dr. Sandra Yuter).

Quantitative precipitation forecasts in extratropical snow storms have long been a challenge and the mechanisms behind enhanced snow fall remains unclear. This study combines radar data from six National Weather Service operational radars to characterize the spatial distributions and variability of precipitation and velocity features from 108 snow storms in the northeast United States between 1996 and 2016.

Snow storms were classified based on the geometry and number of snow bands present throughout their observed life cycle. Single band features are defined as a band of precipitation at least 250 km in length, 20 to 100 km wide, and having an aspect ratio less than or equal to 0.5 for at least one hour. Multi-band features are defined as a band of precipitation less than 250 km in length, 10 to 50 km in width, and having an aspect ratio less or equal to than 0.5 for at least one hour. At least two multi-band features must be identified for a time to be considered multi-banded. Non-banded is any precipitation that does not fall into one of the two previous categories including cellular precipitation or stratiform precipitation. Snow storms with multi-bands were found to be the most common followed by snow storms with coexisting single and multi-bands, snow storms with no band features, and snow storms with only single bands. Most band features were observed to develop and remain in the northern part of the cyclone. Single bands were centered in the northwest quadrant. Multi-bands were primarily found in both the northeast and northwest quadrants.

The weaker, stratiform precipitation tends to form first, then areas of intense snow fall within bands develop. This time sequence differs from a typical deep convective system where heavy precipitation forms first and then weakens to form stratiform precipitation. The storm total band area was found to only represent ~7% of the total precipitation area. The time bands spend over a specific location greatly influences snowfall accumulation.

No clear, sustained convergence signatures were found associated with multi-bands suggesting that these bands do not consist of persistent, active updrafts. Doppler velocity waves were observed in most, but not all storms with multi-bands. We detected the Doppler velocity waves as regions where the radial velocity changes over a short time (between volume scans).Doppler velocity waves were typically ~4 km deep and found to move in a

direction more than 45◦ different than the near surface layer (0-2 km) strongly suggesting that these waves may be gravity waves.

Observed Characteristics of Mesoscale Banding in Coastal Northeast U.S. Snow Storms

By

Nicole Prentice Hoban

A thesis submitted to the Graduate Faculty of
North Carolina State University
in partial fulfillment of the
requirements for the degree of
Master of Science

Marine, Earth, and Atmospheric Science

Raleigh, North Carolina
2016

APPROVED BY:

_____	_____
Dr. Sandra Yuter Committee Chair	Dr. Brian Colle

_____
Dr. Matthew Parker

ACKNOWLEDGMENTS

I would like to thank my advisor, Dr. Sandra Yuter, for her continued support and motivation over these past two years. I would like to thank members of my research group past and present for their technical support, help processes mounds of data, and being wonderful people to work with. I thank Dr. Brain Colle for his continuous guidance in this project from day one, and Dr. Matthew Parker, for providing valuable insight. I would also like to thank my friends and family for their continued support over the past years. Last, I would like to thank my cats for providing much need stress and comic relief.

DEDICATION

I would like to dedicate this thesis to my grandmother. Her example as a strong independent woman gave me the strength and motivation to complete this thesis.

TABLE OF CONTENTS

LIST OF TABLES

LIST OF FIGURES

CHAPTER 1 - Introduction

The northeast United States is a densely populated area and includes the large metropolitan areas of New York City, NY and Boston, MA. Major winter storms in the northeast United States have large societal and economic impacts. Snow and mixed phased precipitation can shut down public transportation, highways, major airports, and key public services (Kocin et al. 1995). This region has been hit by numerous major winter storms in recent years with 2015 setting the record for Boston's snowiest year.

Quantitative precipitation forecasts (QPF) in extratropical cyclones, especially in snow storms, has long been a challenge. A key factor in improving QPF is improving understanding of the physical processes responsible for mesoscale precipitation systems and their predictability (Ralph et al. 2005). Heavy precipitation within extratropical cyclones is often organized into mesoscale bands (Houze et al. 1976; Hobbs 1978; Marks and Austin 1979; Houze and Hobbs 1982; Clark and James 2002). Previous research has shown that QPF in winter storms is sensitive to the occurrence, intensity, and propagation of precipitation bands (Novak et al. 2004; Novak et al. 2008; Novak and Colle 2012). The effects of mesoscale bands are amplified during the cool season when snowfall associated with the bands can produce localized heavy snowfall embedded within relatively lighter snowfall causing extreme snowfall gradients.

Several previous research studies have classified precipitation bands within extratropical cyclones based on the individual band's length, width, intensity, and duration. Houze et al. (1976) used radar observations to survey 11 cyclones affecting western Washington State and identified and defined six types of rain bands: warm frontal, warm sector, cold frontal wide, cold frontal narrow, wave, and postfrontal (Figure 1.1). Houze et al. (1976) provided a template for future band classification schemes to build upon. Novak et al. (2004) used operational radar data to examine and classify bands within cool season extratropical cyclones in the northeast United States. Bands were classified into one of 4 categories: single, multi-, narrow cold frontal, and transitory banded structures. Novak et al. (2004) classified a total of 88 rain, snow, and mixed precipitation storms with banded structures across 5 cool seasons and found single bands to be the most common followed by

transitory, narrow cold frontal, and multi- respectively. Additionally, 13 cases were classified as non-banded. Figure 1.2 illustrates examples of a single and a non-banded case from Novak et al. (2004).

The development of banded precipitation can be attributed to several different processes including slantwise convection, frontogenesis, and mesoscale waves (Gaffin et al. 2002). Emanuel (1985) theorized slantwise convection to be the result of the release of conditional symmetric instability (CSI) in which an air parcel follows an unstable slantwise path in a conditionally and statically stable environment. Schultz and Schumacher (1999) caution that other alternatives should be ruled out before considering CSI. Schultz and Schumacher (1999) also explained that an ingredients-based methodology (moisture, lift and instability) demonstrates that CSI alone is not sufficient to initiate slantwise convection. Novak et al. (2010) found the most probable stability state during band formation to be either weakly stable conditions or conditional instability with CSI being less common.

Well-defined single bands and the mechanisms behind their formation, maintenance, and decay have been the focus of numerous studies (Sanders and Bosart 1985; Sanders 1986; Clark et al. 2002; Novak et al. 2004; Novak et al. 2008, Novak et al. 2010; Stark et al. 2013). Frontogenesis was found to be the primary formation mechanism of single bands in extratropical cyclones. Single bands coincide with the ascending branch of the frontogenetical circulation in environments of weak moist symmetric instability or CSI. Schultz and Schumacher (1999) demonstrated that frontogenesis and CSI are not independent of each other. Novak et al. (2004) showed that single bands most commonly form in the northwest quadrant of extratropical cyclones in an area of deep layer frontogenesis in the presence of small moist symmetric stability. Figure 1.3 is a conceptual model from Novak et al. (2004) of the synoptic environment for a single band and a non-banded cases. Novak et al. (2010) expanded upon Novak et al. (2004) to show midlevel frontogenesis is a key factor in the formation and growth of a large number of single bands. Additionally, Novak et al. (2010) found that frontogenesis nearly doubles leading up to the development of the single band, and once frontogenesis begins to decay the single band dissipates. Stark et al. (2013)

also examined two strong banded cases over the northeast United States that were associated with midlevel frontogenesis.

Several studies have focused on the physical mechanisms that cause the formation and maintenance of multi-bands using idealized models. Few investigators have linked idealized studies to observational data. Xu (1992) used a semi-geostrophic model to investigate the formation and evolution of frontal rainbands in association with dry and moist geostrophic potential vorticity anomalies (MGPV). Xu (1992) found multiple rainbands can be generating from frontal circulations if the MGPV becomes negative. When MGPV is positive, multiple rainbands can only be generated by preexisting MGPV anomalies and maintained through a weak feedback between vertical motion and warming anomalies. Morcrette and Browning (2006) employed a dry idealized numerical model to demonstrate the importance of both CSI and absolute momentum adjustment via inertial instability on the formation of multi-bands. Pizzamei et al. (2005) used a cloud resolving numerical model to find the release of CSI to be less important than propagating density currents associated with downdrafts caused by evaporation cooling of hydrometeors.

Several studies have suggested the importance of upright convective generating cells and their enhancement of the stratiform precipitation field below (Wexler and Atlas 1959; Hobbs 1978; Rosenow et al. 2014). Novak et al. (2008) suggested multi-bands may develop in a region of confluence (frontogenesis). Other studies have stressed the importance of latent heat release and its effects on the underlying cyclone and forcing for precipitation. Davis and Emanuel (1991) discussed how the release of latent heat due to precipitation/convection aids in the development of potential vorticity (PV) anomalies near the surface leading to enhanced cyclogenesis. Additionally, Novak et al. (2009) demonstrated how frontogentical forcing for banding is highly sensitive to upstream PV modification from precipitation.

Gravity waves have been shown to trigger and enhance convection (Mapes 1993; Gaffin et al. 2002; Fovell et al. 2006, Allen et al. 2012) and latent heat release is a known trigger for gravity waves. Other studies have examined gravity waves trigger by other mechanisms and their effects on precipitation. Gaffin et al (2002) demonstrated how gravity waves initiated by mountainous flow triggered a banded heavy snow event over the southern Appalachian

region. Allen et al (2012) showed how gravity waves triggered by geostrophic readjustment affected a region of marine stratocumulus. Fovell et al. (2006) demonstrated how gravity waves caused by latent heat release inside a squall line caused precipitation to form ahead of squall line (action at a distance).

This study utilizes data from six weather radars to obtain a large spatial coverage of snow storms over the coastal northeastern United States. The areal extensive weather radar coverage in the northeast United States allows us to observe the evolution of snow storms and the life cycles of snow bands associated with extratropical cyclones. Many studies have used observations and modeling to examine case studies of east coast winter storms (Novak et al. 2008; Stark et al. 2013; Picca et al. 2014). Multi-season analyses are fewer (Novak et al. 2004; Novak et al. 2010; Colle et al. 2014). The mechanisms for the formation and maintenance of multi-bands in coastal northeast United States remain unclear and could be caused by some combination of convective generating cells, confluence associated with frontogenesis, and gravity waves. To our knowledge, this is the first study to use multi-decade radar data to examine mesoscale precipitation bands, including multi-bands, in combination with analysis of associated kinematic structures within the U.S. east coast snow storms. This study uses a 20 year data set comprising 108 snow storms in the northeast US to:

- Address and quantify the inter-storm variability of snow band structures and their context within the larger cyclone.
- Examine potential mechanisms behind the formation and maintenance of multi-bands, especially dynamical signatures observable with Doppler radial velocity.

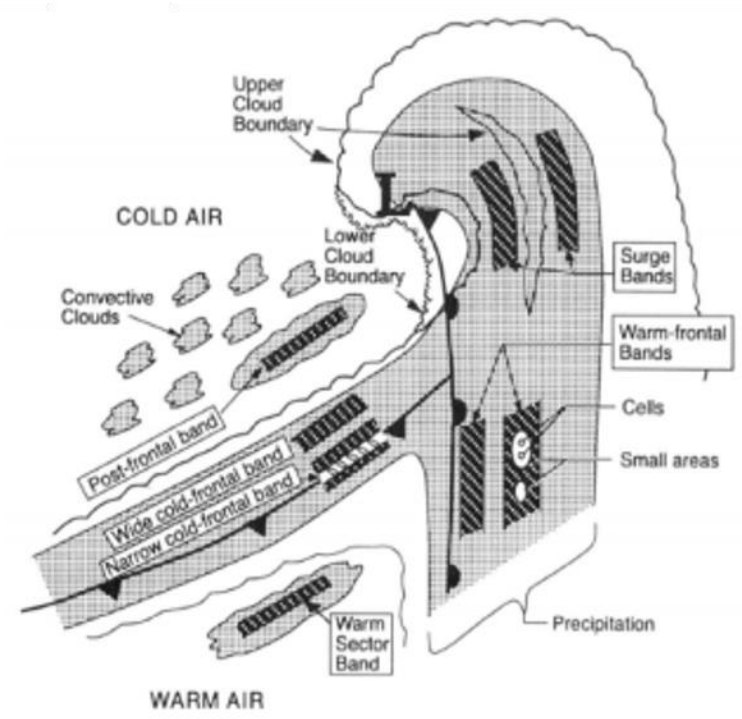

Figure 1.1 Idealized conceptual model of clouds, precipitation and rain bands associated with an extratropical cyclone (from Houze 1993)

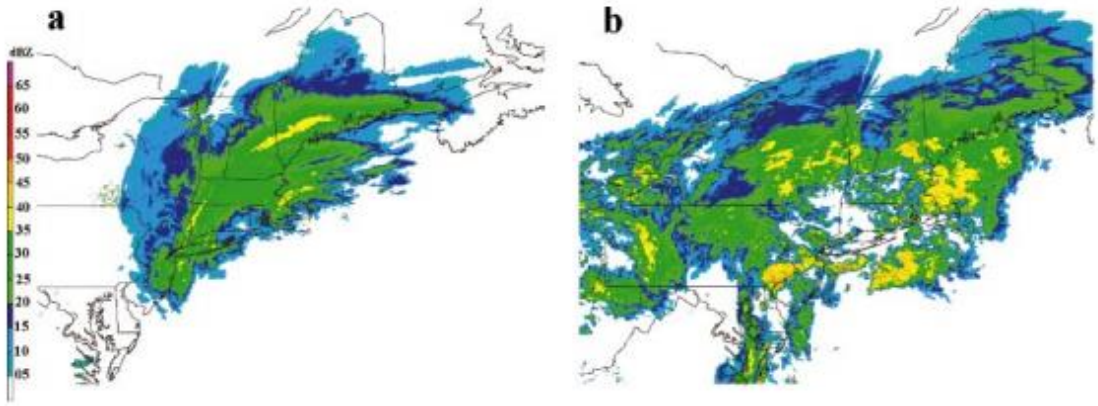

Figure 1.2 WSR-88D radar mosaic of (a) a single banded event valid at 0000 UTC 6 Feb 2001 and (b) a non-banded case valid at 1200 UTC 14 Feb 2000. Color scale along left side is partitioned every 5 dBZ (from Novak et al. 2004).

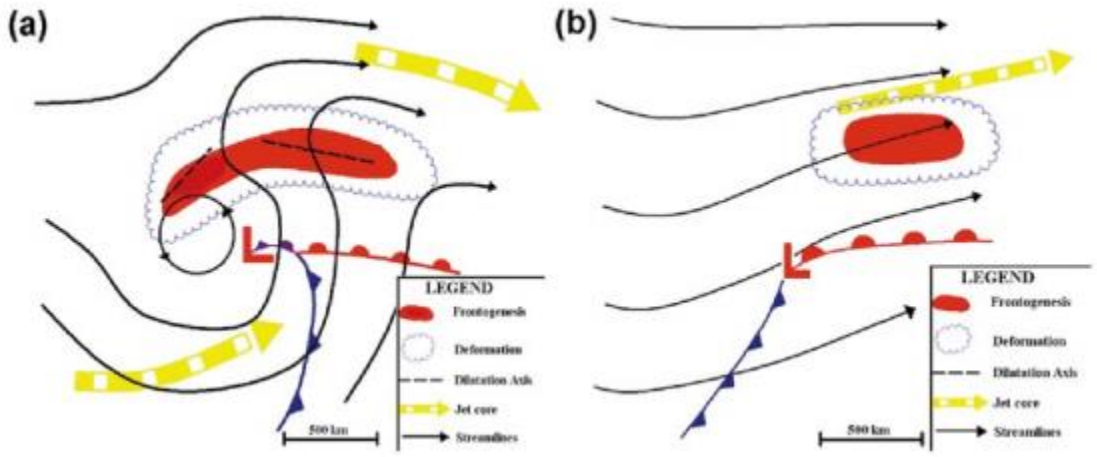

Figure 1.3 Conceptual model of the synoptic and mesoscale flow environment associated with (a) a single banded event and (b) a non-banded case highlighting the key features. Features shown include midlevel frontogenesis (red shading), midlevel deformation zone (encompassed by scalloped blue line) and associated primary dilation axes [dashed lines in (a)], midlevel streamlines (black lines), and upper-level jet cores (wide dashed arrows) (from Novak et al. 2004).

CHAPTER 2 – Data/Methods

The area of interest for this study spans the coastal northeast United States from Delaware to the southern coast of Maine with a particular focus on the corridor between New York City and Boston (Figure 2.1). This study utilizes data from six National Weather Service (NWS) operational Weather Surveillance Radars-1988 Doppler (WSR-88D, Crum et al. 1993) to observe characteristics of wide spread snow storms.

2.1 Snow Storm Definition

For this study, a snow storm is defined as producing at least 1 inch of snow within a 24 hour period at 2 of 7 Automated Surface Observing System (ASOS) stations across the northeast United States. The ASOS stations are located at: Portland, Maine, Islip, New York, Boston, Massachusetts, Philadelphia, PA, Bridgeport, CT, Providence, RI, and Newark, NJ (Figure 2.1). This definition selects widespread, impactful snow storms. 108 storms were identified during the cool season (October to March) from 1996 to 2016. The 108 storms includes several snow storms with significant precipitation banding over the ocean. Appendix A provides detailed information on the timing of each of the 108 storms. Note that many of the snow storms also contained radar echo with mixed precipitation and rain, particularly in the warm sector of the cyclone. We take several steps, described below, to focus our analysis on the portions of the precipitating area where snow is likely falling at the surface.

2.1 Radar Data

Data from six NWS WSR-88Ds were analyzed in this study. The six radars are located at: Portland, Maine (KGYX), Albany, New York (KENX), Boston, Massachusetts (KBOX), Long Island, New York (KOKX), Mt. Holly, New Jersey (KDIX), and Dover, Delaware (KDOX) (Figure 2.1). When combined, these radars offer a regional picture of precipitation along much of the northeast US coast. Archived Level II data was obtained from the National Center for Environmental Information (NCEI) Next Generation Radar (NEXRAD) Data Inventory (NOAA 1991) for 108 snow storms (198 days). These observations provide a large, nearly continuous data set with volume scans every 6 to 10

minutes. Since the majority of this study period was prior to the dual polarization upgrade, no polarimetric data was used.

2.2.1 Quality Control

Level II polar coordinate radar data from each radar was quality controlled using similar methods to Yuter (2011), Cunningham and Yuter (2014) and Corbin (2016). A clutter map for each radar was designed to eliminate data points that consistently return high reflectivity values even in clear conditions. The clutter map also removes data within 2 km of each radar as these regions have high concentrations of non-meteorological echoes (Figure 2.2). For a detailed description of clutter removal, see Appendix B of Corbin (2016). In regards to beam blockage, KDOX, KDIX, and KBOX all have unblocked clear views of their surrounding areas. KENX and KGYX have some beam blockage due to surrounding mountains, and KOKX has one point of beam blockage to its northwest from a nearby water tower.

Following the methods detailed in Corbin (2016), a relative radar reflectivity calibration was determined from Level II data for each of the 108 snow storms. KOKX was used as the base radar and relative offsets in dB were determined for the other 5 radars. The 200 km radius radar domains of KBOX, KENX, and KDIX overlap with KOKX. KDOX was calibrated relative to the corrected KDIX data. KGYX was calibrated to corrected KBOX data. For a detailed descriptions of the radar calibration methods see Appendix C of Corbin (2016).

Radial velocities in Level II polar coordinate radar files for each radar were dealiased (unfolded) using an unfolding algorithm in the Python-ARM Radar Toolkit provided by Jonathan Helmus (Helmus et al. 2016).

2.2.2 Microphysics Fields

Differing from Cunningham and Yuter (2014) and Corbin (2016), reflectivity data from the two lowest elevation angles in the radar volume scan (0.5° and 1.5°) were combined to form two-dimensional Cartesian maps using the National Center for Atmospheric

Research (NCAR) REORDER software (NCAR 2012). Data from a single radar was interpolated to a 400 x 400 km^2 grid with horizontal grid spacing of 2 km. The interpolation was performed using a Cressman weighting scheme with an azimuthal radius of 1.1° and an elevation radius of 1 km.

To achieve more visual separation between snow bands and to allow for more subtle banding to stand out, reflectivity was rescaled to an estimated snow rate. Snow rate can vary significantly based on particle number, snow crystal type, snow density, and the amount of riming present making determining an exact relationship between snow rate and radar reflectivity difficult (Rasmussen et al. 2003). We use the relationship from Rasmussen and Dixon (2003), $Z_e = 57.3S^{1.67}$, where Z_e is equivalent radar reflectivity and S is snow rate in mm/hr. We are not using snow rate to estimate the amount of precipitation, but simply as a way to rescale the reflectivity to estimated values that linearly scale with snow rate.

2.2.3 Detection of Snow Bands Relative to Surrounding Precipitation

We distinguish snow bands from the surrounding weaker radar echo by use of a convective/stratiform (convsf) algorithm that assesses the relative peakedness of a pixel value compared to the values of surrounding pixels. In our use for this research, snow bands have roughly similar relative reflectivity characteristics compared to the surrounding precipitation as convective precipitation does to stratiform precipitation. We use the estimated snow rate field as input to the convsf algorithm since the bands are more distinct in snow rate as compared to radar reflectivity. The convsf algorithm was originally defined by Churchill and Houze (1984) and has been adapted by Steiner et al. (1995), Houze (1997), Yuter el al. (2005) and Cunningham and Yuter (2014) for various radar and storm characteristics. The algorithm characterizes every pixel in a two-dimensional gridded data field as either convective, stratiform, or weak echo. The convsf algorithm was originally develop for the tropics and must be tuned for a particular radar, geographic region, and weather regime. As part of tuning the algorithm for this application, we turned off the convective threshold value and relied on the detection of peakedness (sharp gradients) within the reflectivity field following Yuter and Houze (1997) and Cunningham and Yuter (2014).

Due to the typical lower reflectivity values of snow, the weak echo criteria was turned off and any echo not identified as convective was identified as stratiform. The algorithm was tuned and tested on several cases to make sure it was correctly identifying areas of locally intense snowfall (Figure 2.3, Animation 2.3). Test cases were tuned to make sure the algorithm was identifying the proper area of precipitation bands and there was enough separation between bands while still capturing the entire area of connected locally-enhanced precipitation. We will use the terms "band" and stratiform, rather than convective and stratiform in this thesis to refer to the output of the convsf algorithm based on the estimated snow rate input. The long history of use of the term "convective" precipitation in the mesoscale convective system literature (e.g. Houze 1997) has connotations that may or may not be appropriate for the locally enhanced snow rates examined in this study, hence, we use the more descriptive term "band".

2.2.4 Snow Band Classifications

The nature and geometries of relative precipitation variations throughout the life cycle of each snow storm were classified manually as either a single band, multi-bands, or non-banded following Ganetis et al. (2015) which in turn is based on Novak et al. (2004). Single band features are defined as a band of precipitation at least 250 km in length, 20 to 100 km wide, and having an aspect ratio less than or equal to 0.5 for at least one hour. Multi-band features are defined as a band of precipitation less than 250 km in length, 10 to 50 km in width, and having an aspect ratio less or equal to than 0.5 for at least one hour. At least two multi-band features must be identified for a time to be considered multi-banded. Non-banded is any precipitation that does not fall into one of the two previous categories including cellular precipitation or stratiform precipitation. We acknowledge that long band and short bands would be more intuitive definitions for single and multi-bands as more than one single band can occur at a time and multi-bands as simply smaller bands; however we chose to keep the same nomenclature are the previous studies in which our definitions are based on (Ganetis et al. 2015, Novak et al 2004).

Each storm was in turn classified based on the type of bands present throughout its life cycle as single banded, multi-banded, coexisting single and multi-banded, or non-banded. Single banded storms are defined as having a single band and less than or equal to 2 multi-bands. Multi-banded storms have no large primary band and greater than 3 multi-bands. Single and multi-banded storms have both a single band and greater than 3 multi-bands present at some time during the life cycle of the storm. In all snow storms classified as having coexisting single and multi-bands, single and multi-bands were found to be present together for at least a portion of the storm duration. In these same storms, there were also times prior to the formation of the single band with just multi-bands present. However, these coexisting single and multi-band snow storms did not have times with single bands and no multi-bands. Non-banded is defined as no banded structures throughout the life cycle of the storm.

2.2.5 Composite Frequency of Precipitation for all Storms

As an initial step in the analysis, we wanted to determine where preferred areas for precipitation occurred in the northeast U.S. to understand the base state represented by all storms. Precipitation enhancement may occur related to local circulations associated with hills and land/ocean boundaries (Colle and Yuter 2007). Following the methods of Yuter et al. (2011), Cunningham and Yuter (2014), and Corbin (2016) but combining the lowest two tilts (0.5° and 1.5°), we created precipitation frequency of exceedance maps for each radar and each snow storm. Precipitation frequency of exceedance maps describes the frequency or amount of time a grid cell reports moderate or heavier precipitation relative to the number of volumes per event. A grid cell is considered to be at least moderately precipitating when radar reflectivity is greater than or equal to 13 dBZ or a snow rate between 0.1 to 0.5 mm/hr snow water equivalent depending on the density of the snow.

Precipitation frequency of exceedance maps from each radar were stitched together and regridded to an 801 km by 801 km regional precipitation frequency map with horizontal grid spacing of 2 km. Overlapping data points were assigned the highest precipitation frequency of exceedance value intersecting that grid point. All 108 snow storms were

aggregated into one master precipitation frequency composite (Figure 2.4). Table 2.1 shows the total number of storm hours for each radar. KOKX has the highest amount of storm hours and is used as the base radar for which the other are compared. KDOX was excluded from this composite as it only has 62% of the hours compared to KOKX yielding lower values of precipitation frequency. KDOX is located at Dover Air Force Base and data from 2000 to 2005 was not released to the public. The master composite demonstrates fairly even values of precipitation frequency of exceedance throughout our domain and there is no apparent preferred or topographically enhanced precipitation area in the region. The radar-concentric patterns are expected since at farther ranges the beam altitude is higher and reflectivity values typically decrease with increasing height. The lack of any signatures related to hills or coastlines is likely a consequence of varying wind directions in the region during the winter season. Over the 108 storms, any preference for precipitation on the windward side of hills during a particular storm or a period within a storm is washed out as the wind direction (and windward side) shifts.

2.3 Velocity Band Detection

To isolate waves seen visually in radial velocity data movies, two sequential radial velocity fields in polar coordinates were subtracted to get a difference field. The difference field contains banded features with both a negative and positive values that represent a temporal change in the radial velocity field (Figure 2.5, Animation 2.5). Figure 2.5a and Figure 2.5b represent two consecutive times and Figure 2.5c is the resulting difference field when they are subtracted. To achieve better separation between nearby velocity bands, the difference field was converted to a binary field with the negative portion of the difference field was given a one and the positive portion was given a zero (Figure 2.5d). The binary field was then interpolated to a 1 km x 1 km Cartesian grid. Any group of pixels or blobs that contained 3 pixels or less were removed to reduce noise. Figure 2.6 is a vertical cross-section schematic that shows the speed acceleration and deceleration detected in the Doppler velocity temporal difference field. Positive values of speed acceleration (time 2 speed > time 1 speed) represent areas of divergence and inferred downward motion and negative values represent

areas of deceleration and associated convergence and inferred upward motion. Since we are using only the negative portion of the difference of radial velocities in time 2 minus those in time 1 (Figure 2.5d), we are identifying areas of localized speed deceleration and associated convergence and inferred upward motion as velocity bands. We chose to use a temporal difference field rather than an instantaneous convergence/divergence field as it is more reliably sampled by the radar. Instantaneous convergence/divergence is calculated along each radial meaning that if the convergence/divergence is not happening nearly perpendicular to the radar beam, it will not be observed.

There is the potential for aliasing or waves moving their wavelength in between radar scans. Doppler velocity waves demonstrated wavelengths ranging from 10-30 km and speeds from 10.4-36.3 m/s (wavelengths were manually calculated and wave speed calculations are discussed in section 2.4). Assuming a time difference of 5 minutes between each radar scan, according to the observed speeds a wave will travel between 3.1 and 10.9 km. If a wave is traveling at the maximum observed wave speed (36 m/s) for this study, it is possible that it could travel one approximately 10 km between radar scans. However, only three storms with waves moving approximately 36 m/s were observed and the waves in those cases had wavelengths of at least 15 km. While aliasing is possible, we do not believe it to be a significant problem for this study.

2.4 Wave and Snow Speed

Wave speed was calculated by extracting the geometric transformation or the average pixel translation between two consecutive images using the Matlab function imregtform. Given the average pixel translation, the kilometer scale of each pixel, and the time between each image or radar volume, an estimate of the speed of the waves between two consecutive radar volumes was made. Boxes of 1º longitude by 2º latitude were picked for various times during each storm that exhibited waves. Areas chosen focused on regions with both waves and multi-bands. An average wave velocity speed and direction was estimated for two hour windows. The same methods were used to estimate snow band speed over the same boxes and time frames using the estimated snow rate field as input. Previous research (Sanders and

Bosart 1985; Sanders 1986; Clark et al. 2002; Novak et al. 2004; Novak et al. 2008, Novak et al. 2010; Stark et al. 2013) has shown that single bands are associated with areas of frontogenesis and deformation which are known to slow the movement of band features.

2.5 Stitched Regional Maps

Following the methods of Corbin (2016), radar fields for each scanned volume from individual radars were stitched together and interpolated to an 801 km by 801 km regional map with horizontal grid spacing of 2 km. Volume scan start times do not line up among the 6 radars precisely. KOKX was used as the central radar and stitched regional maps were assigned its radar volume time. Data from the 5 other radars were used as long as their time was within 8 minutes of the KOKX time. Some stitched regional maps are missing data from individual radars if the associated data were not available in the archive. Stitched regional maps were made for reflectivity, snow rate, convsf output, and velocity differences. Where radar data from nearby radars overlapped, reflectivity, snow rate, and convsf were assigned the highest value intersecting each grid point. The velocity difference maps were stitched differently from the other variables. In overlapping regions, only data from the southernmost radar was used to mitigate differences from varying volume start times between radars.

Images were made with the available radar data for the complete duration of each of the 108 storm for reflectivity, snow rate, convsf output, and velocity differences (Figure 2.3, Animation 2.3). Images were animated together to make stitched regional movies and can be viewed at our perusal page (precip.meas.ncsu.edu/neus/perusal). These movies allow us to see the evolution of each snow storm and the structures of the precipitation that forms throughout its life cycle. They also allow us to detect whether or not any waves were present during the life cycle of a snow storm.

2.6 Satellite Data

Merged Infrared (IR) satellite data from NASA Tropical Rainfall Measuring Mission ancillary dataset from the Climate Prediction Center, National Center for Environmental Prediction, and the National Weather Service (Janowiak et al. 2001) was used. The merged

IR, which has 4 km x 4 km horizontal resolution with updates every 30 minutes, was subset to the northeastern United States. Merged IR was available from 2000 to 2016 and was used to provide context for the radar data in terms of the evolving cloud shield. Images were plotted for the duration of each snow storm and animated together to get movies of the merged IR satellite data for each snow storm.

2.7 Synoptic Analysis

Surface analysis maps from the NWS/NCEP Ocean Prediction Center (http://nomads.ncdc.noass.gov/ncep/NCEP) were used to assess the location of the surface cyclone, the stage of the cyclone for a given time, and the location of the frontal boundaries. Surface analysis maps from the Ocean Prediction Center were available for 86 of storms out of 108. For the remaining 22 storms, surface analysis maps were obtained from Colorado State University's surface analysis archive and UNISYS surface analysis archive.

The surface analysis maps were used to classify the general synoptic conditions related to a given storm as either simple synoptic or complicated synoptic. Simple synoptic was characterized by a clearly defined low pressure center with a defined cold front, warm front or stationary front, and in many instances, an occluded front. Simple systems correspond to the idealized Norwegian cyclone model (Ahrens and Henson 2016; Schultz and Vaughan 2011). All other synoptic conditions were classified as complicated synoptic. Examples of complicated synoptic situations include: the presence multiple of nearby lows, non-distinct lows, and fronts without nearby lows. Out of the 108 snow storms, 68 storms were classified as simple synoptic and 40 as complicated synoptic

The surface analysis maps were also used to classify the extratropical cyclones associated with each snow storm as either developing or mature. A cyclone was classified as mature if it developed an occlusion at any time during the life cycle of the storm. If a storm did not develop an occlusion, it was classified as developing. Schultz and Vaughan (2011) pointed out that "many cyclones continue to deepen after an occlusion or never occlude at all". An in-depth synoptic analysis for each of the 108 storms was beyond the scope of this

work. Use of the presence of an occluded front to determine storm stage acknowledges that the stage of development of some storms will be misclassified.

2.8 Reanalysis

Three-dimensional gridded data from the NCEP North American Regional Reanalysis (NARR) with 32 km grid spacing (Mesinger et al. 2006) was used in this study to determine the location of the cyclone centers. NARR reanalysis data was available every 3 hours, and the analysis time closest to start and end time of the snow storm and all times in between were used.

The cyclone center was defined to be the lowest mean sea level pressure (MSLP) within close proximity to the northeast US. The cyclone low center was found in 3 hourly NARR surface pressure fields over the duration of each snow storm using Matlab. A line was drawn connecting each location of the cyclone center for the three hour intervals and a smoothing technique applied to obtain a track for each of the 108 snow storms. Fourteen of the low centers were too weak and disorganized during their entire duration in the radar domain to be trackable. Often during the initial stages of the storm development, the low center was not sufficiently strong and distinct to be trackable. Hence, the track information represents the portion of the period when the storm was within the radar domain and when the low was well organized. A few times, the low was not trackable due to weakening and broadening of the low center associated with storm demise. Out of the 94 storms with trackable lows, 54 were tracked for their entire duration in our domain and 40 were tracked for a portion of their duration in our domain. A total of 2250 out of the available 2848 hours (79%) had trackable lows.

2.9 Lagrangian Movies

Using the cyclone center and cyclone tracks defined in section 2.8, we defined a cyclone centric coordinate system to obtain a Lagrangian point of view with respect to the cyclone center. Stitched images of snow rate and of waves in the cyclone-centric coordinate system were made for the entirety of each of the 108 storms (Figure 2.7, Animation 2.7) and

animated together to make regional stitched Lagrangian movies (precip.meas.ncsu.edu/neus/perusal). Compared to a geographic framework where storm evolution and movement are both present, the Lagrangian view permits us to more easily determine where the snow bands and velocity waves are located in relation to the cyclone low, if they have a preferential quadrant relative to the low, and their motion relative to the low.

2.10 Band and Stratiform Precipitation Areas

Using the cyclone tracks defined from reanalysis data, the domain was divided into cyclone quadrants (northwest, northeast, southwest, and southeast) for times when cyclones were trackable. The precipitation area and type of precipitation (band or stratiform) for each quadrant was determined. The percentages of precipitation area that are within a band or stratiform were calculated for each quadrant. Times of mixed precipitation or rain were manually identified and excluded from these calculations.

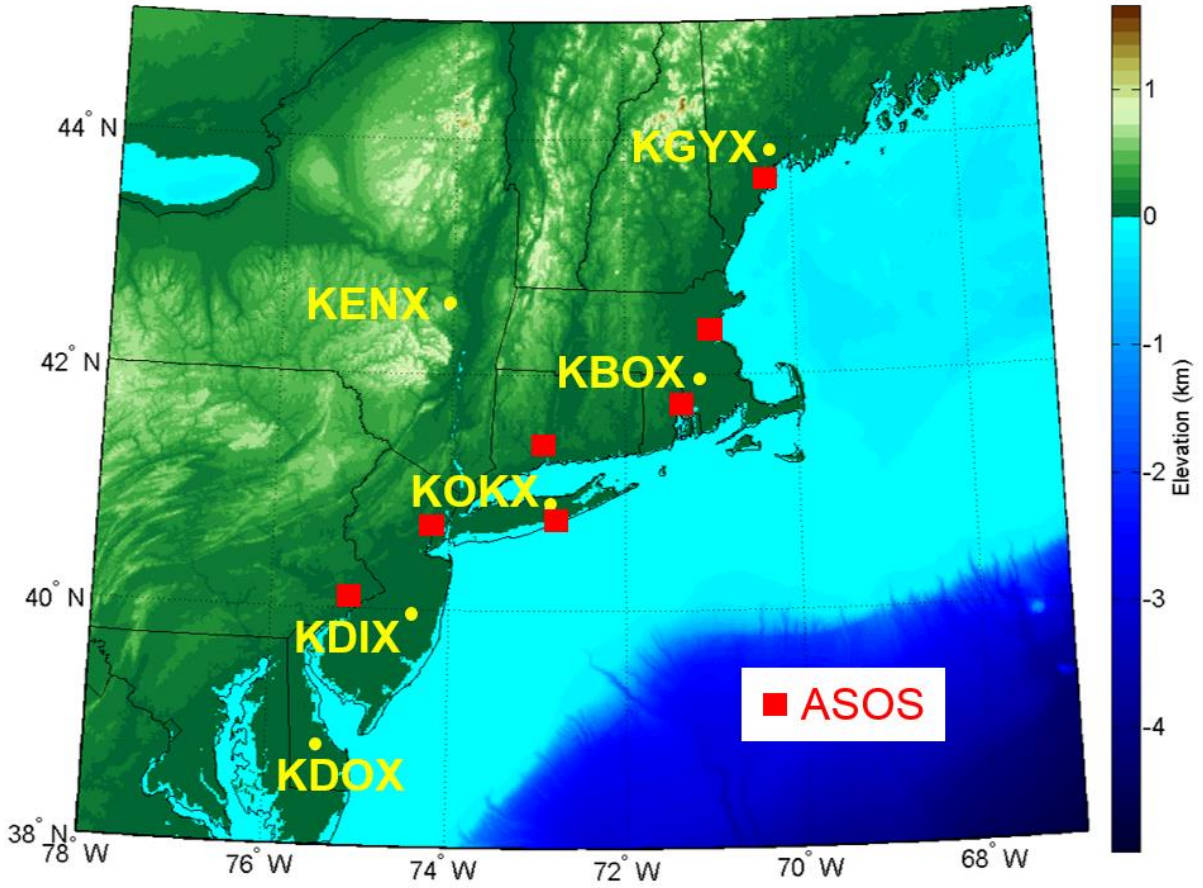

Figure 2.1 Topography of the northeast United States showing the location of the six NWS WSR-88Ds (yellow labels and dots) and the seven ASOS (red squares).

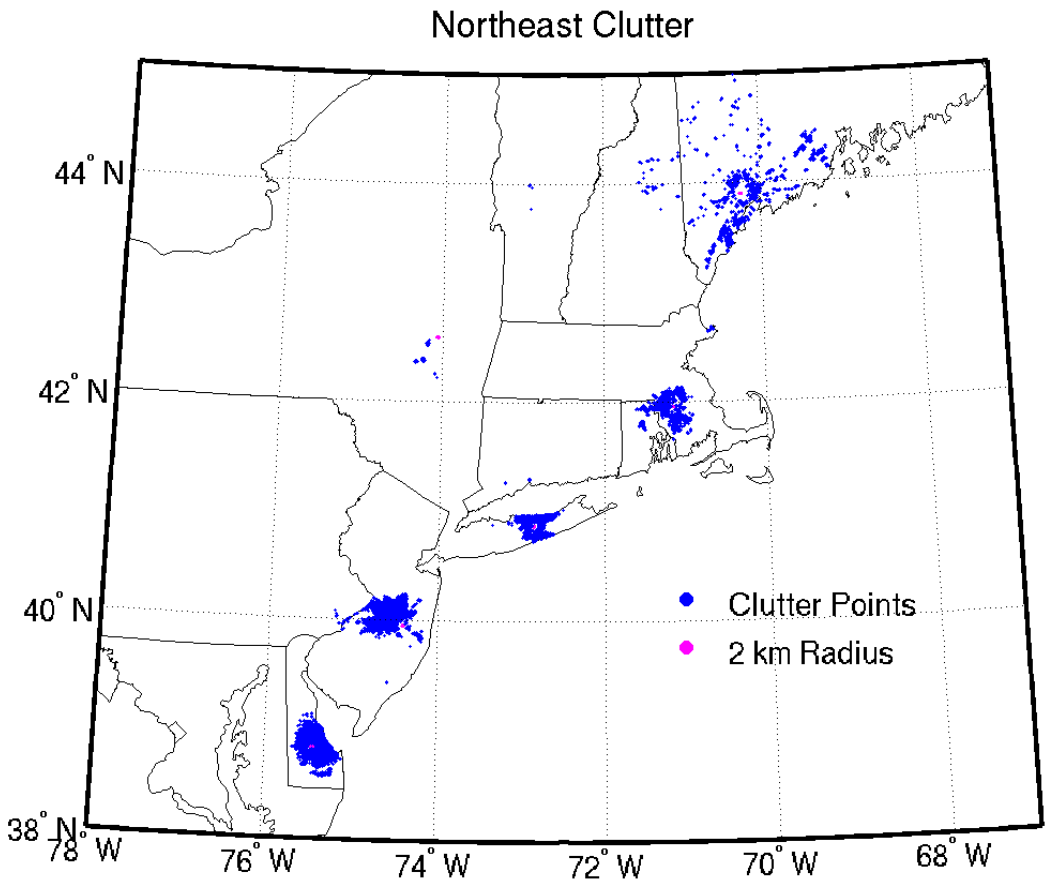

Figure 2.2 Pink dots represent the 2 km radius directly surrounding each radar. The blue dots denote clutter points removed due to persistent non-meteorological echo.

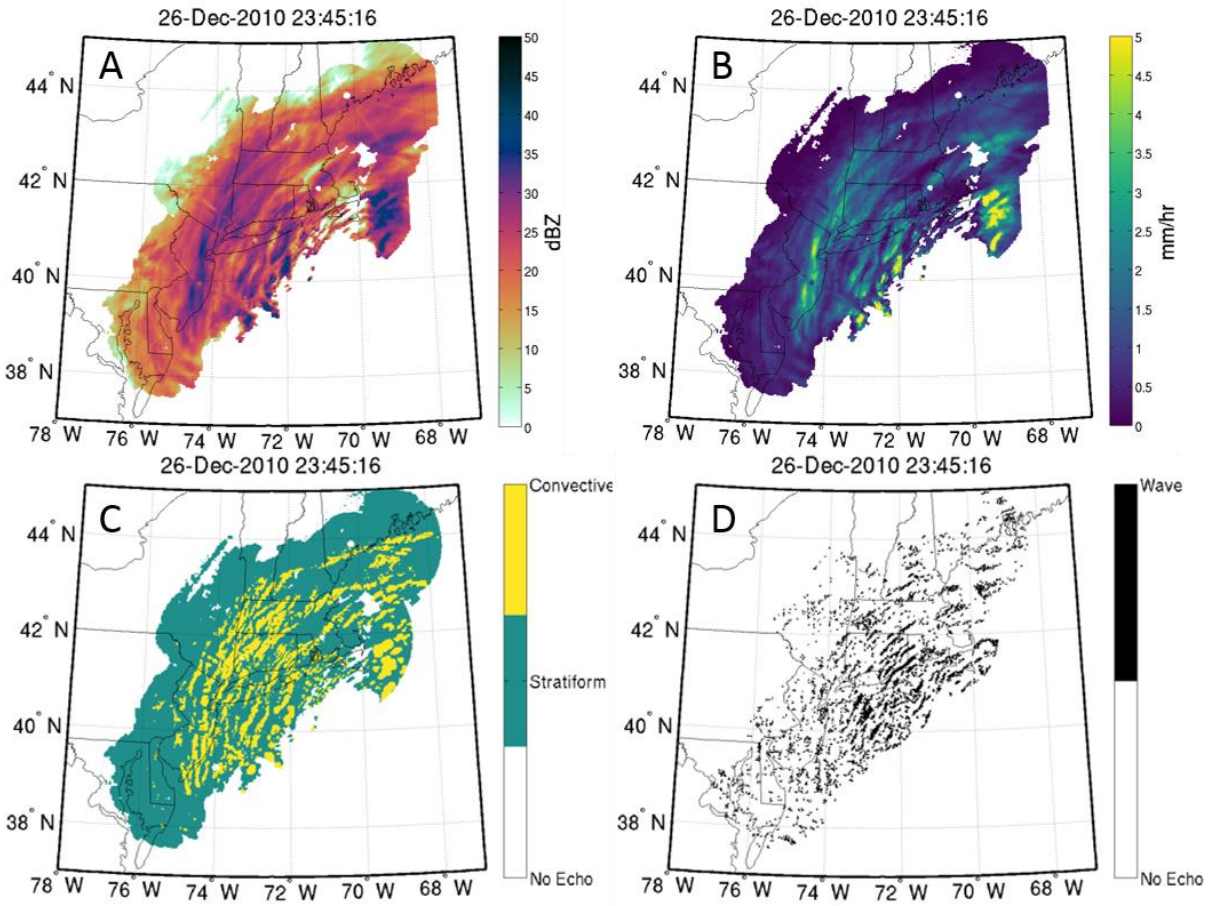

Figure 2.3 Examples of stitched regional maps for reflectivity (A), snow rate (B), convsf output (C), and velocity perturbations (waves) (D).

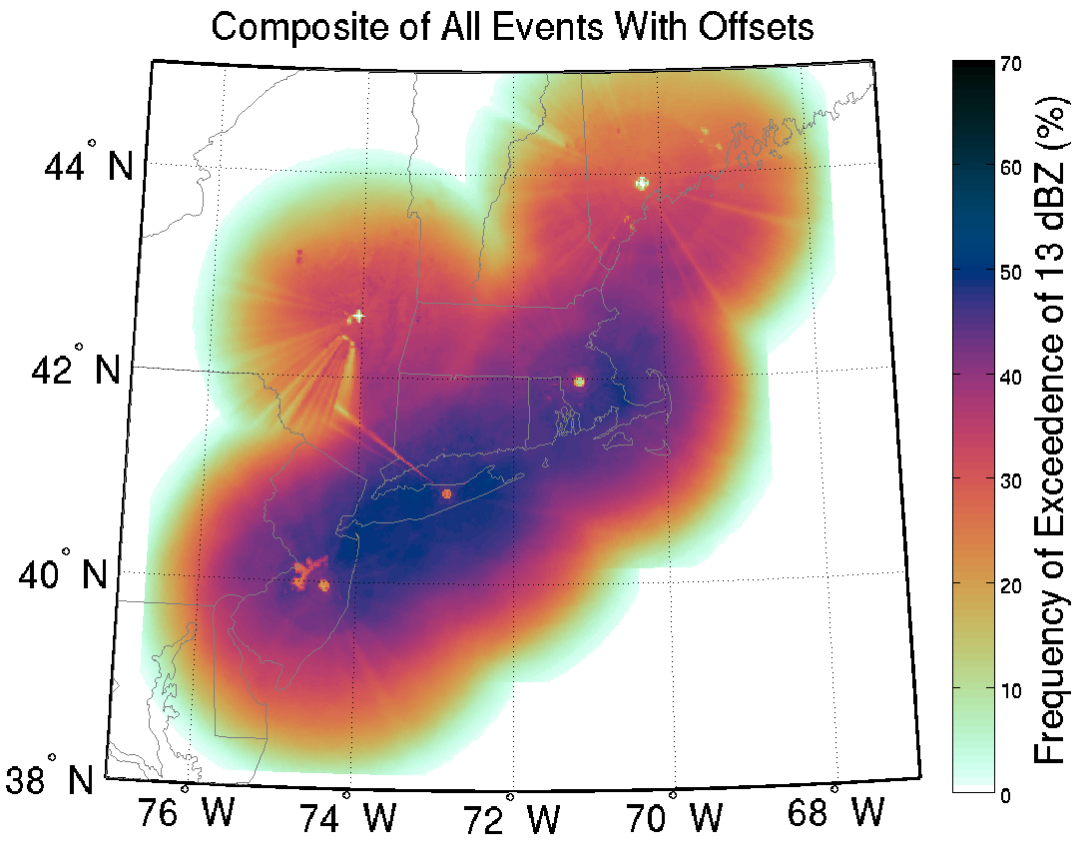

Figure 2.4 Precipitation frequency of exceedance composite for all 108 storms for 5 out of the 6 radars. KDOX is excluded from the composite since data were available for only 62% of the hours relative to those available for KOKX. Shading represents the percent of the hours available that report a value of 13 dBZ or greater.

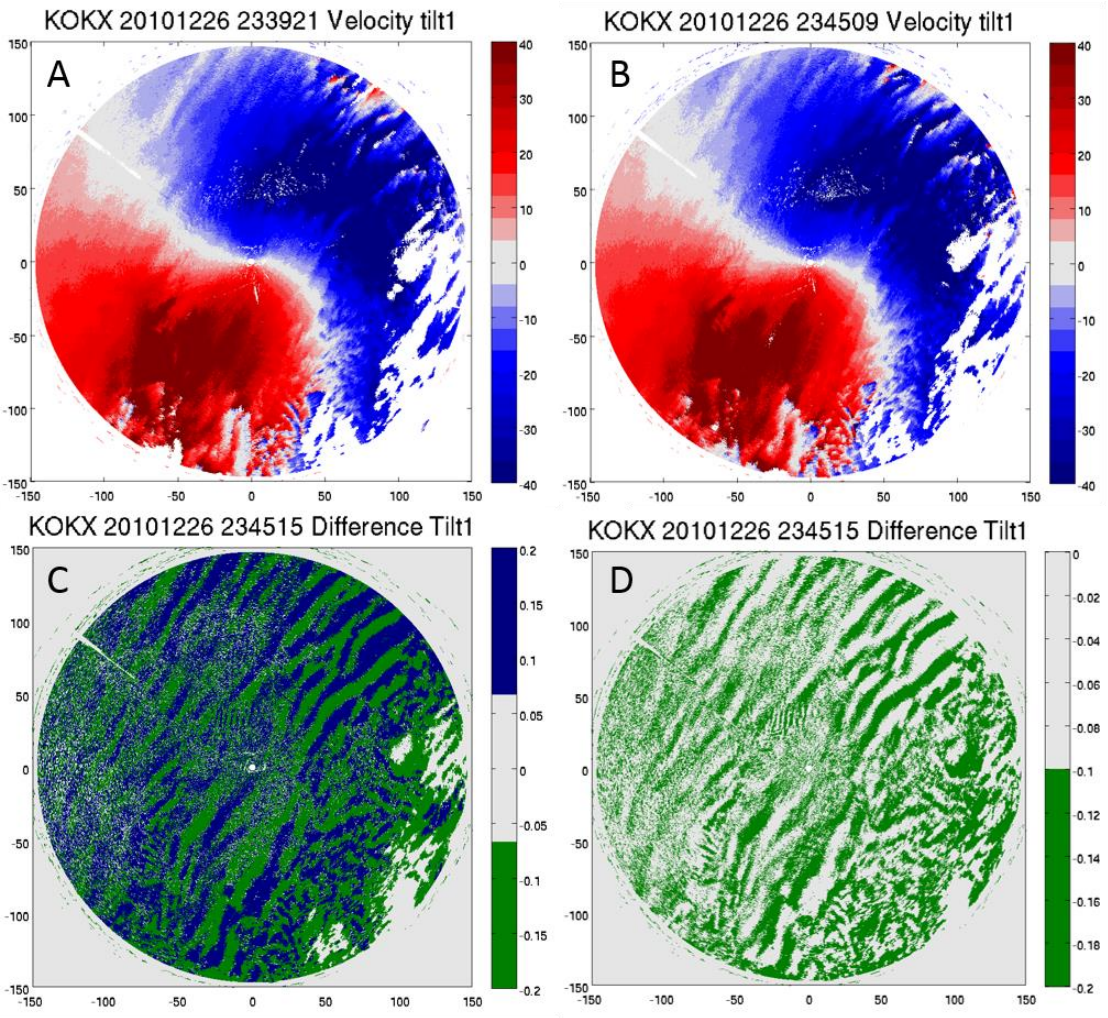

Figure 2.5 A and B) Example of 2 sequential radar velocity fields (polar coordinates). C) The difference field showing both positive and negative temporal velocity changes. D) Only the negative portion of the difference field.

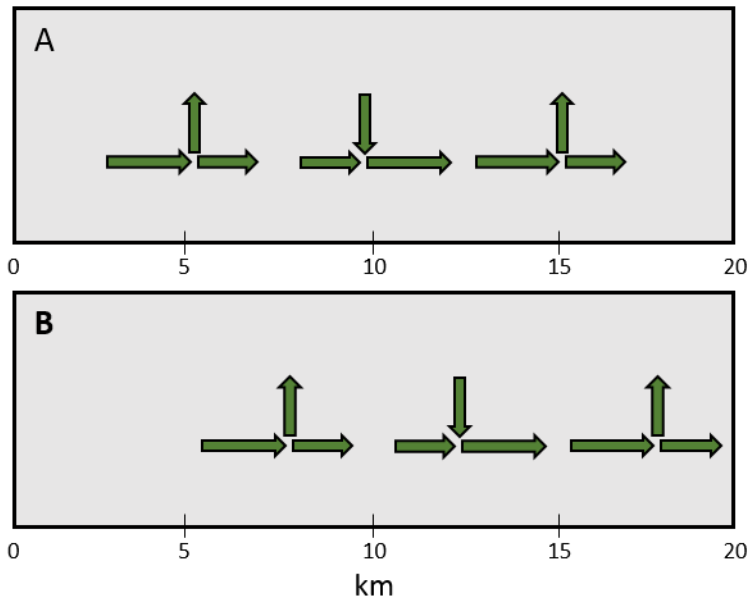

Figure 2.6 A) A vertical cross section schematic of the speed declaration and acceleration detected through the Doppler velocity band detection method and the inferred upward and downward motion. B) as in A) but a 2 minutes later (based on an average Doppler velocity wave speed of 21 m/s).

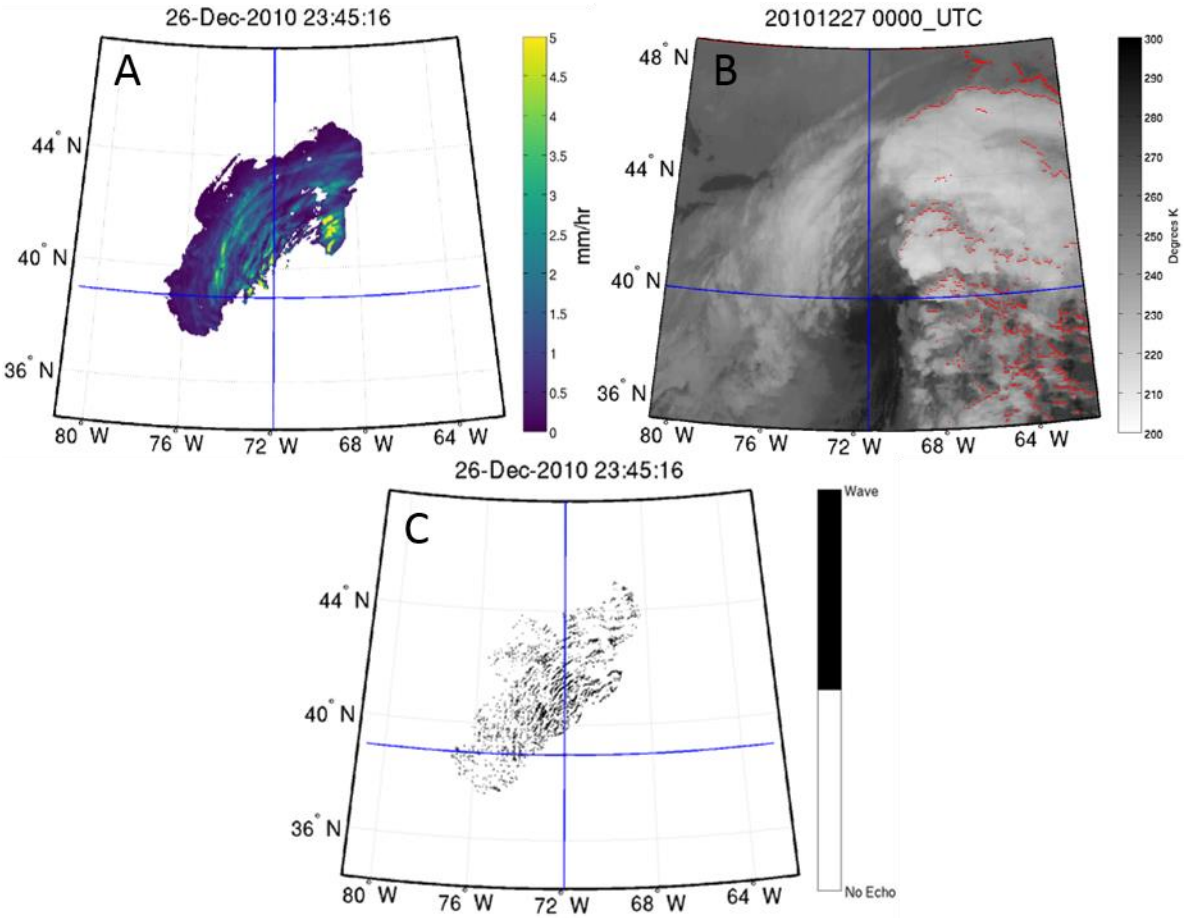

Figure 2.7 Examples of stitched regional maps in Lagrangian framework for snow rate (A), satellite (B), and waves (C).

Table 2.1 Total hours of data available for each radar for the frequency of exceedance master composite.

Radar	Totals Hours of Active Storm Data	Percent of Matching Hours to KOKX
KOKX	2056	100 %
KBOX	1990	97 %
KDIX	1905	93 %
KENX	1885	92 %
KGYX	1797	87 %
KDOX	1277	62 %

CHAPTER 3 – Results

3.1 Synoptic Overview

Each snow storm was classified based on the synoptic front configuration, stage of development, and presence of cold and warm fronts while the storms were within the radar domain (Table 3.1). More of the snow storms (68) were found to have simple synoptic conditions (Norwegian cyclone model) as compared to more complicated synoptic conditions (40). Of the 108 snow storms, 98 snow storms had warm fronts associated with them (91% of snow storms) and 103 snow storms had cold fronts associated with them (95% of snow storms). Each cyclone was also subjectively classified based on its observed cyclogenesis stage (Bjerkness and Solberg 1922) using the 6 hourly surface analysis maps available throughout the duration of the snow storm. While within the radar domain, 63 snow storms reached maturity including the presence of an occlusion (58% of storms) and the rest either did not develop an occluded front or did not have a defined low pressure center associated with them.

3.2 Cyclone Tracks

For periods when the low was of sufficient strength in the NARR reanalysis to be tracked (Section 2.8), cyclone low centers tended to first appear near the southern border of our radar domain around Cape Hatteras, NC and track toward the northeast (Table 3.2a). The majority of low centers remained over the ocean, some tracked from land to the ocean, and others hugged the northeast coast line (Table 3.2b). Of the 94 snow storms with well-defined low pressure centers, 76 snow storms (80% of snow storms) moved to the northeast, 15 snow storms (16% of snow storms) moved to the east, and 2 snow storms (2% of snow storms) moved to the southeast (Table 3.2a).

3.3 Snow Band Characteristics

Following the classification methodology of Ganetis et al. (2015), the snow storms were categorized according to what types of snow bands (single band, multi-bands only, coexisting single and multi-bands, and non-banded) were present during the storm's duration

in the radar domain (Table 3.3). Storms with only multi-bands were found to be the most common type with 39 snow storms (36% of storms). Coexisting single and multi-bands were found to be the second most common type with 32 of the snow storms (30% of snow storms). Storms categorized as coexisting single and multi-bands contained a period where single bands and multi-bands co-occurred. The lifecycle of these storms varied and included multi-bands merging into preexisting single bands, and single bands breaking up into multi-bands. Thirty snow storms (27%) were stratiform only and had no clear band feature throughout their life cycle. Snow storms with only a single bands were the least common storm classification with only 7 snow storms (7% of snow storms).

These results differ strongly from Novak et al.'s (2004) examination of 88 snow, mixed precipitation, and rain storms during the cool season where single bands were found to occur in 48 out of 75 storms with bands (27 storms had multi-bands and 13 were non-banded). The classification of the band geometries is similar between this study and Novak et al. (2004) since the Ganetis et al. (2015) method is based on Novak et al.'s (2004) method. The COMET radar reflectivity mosaic used by Novak et al. (2004) is presented in their paper with a color scale with 5 dB steps. If indeed the reflectivity values in the COMET mosaics were simplified to the nearest 5 dB, more subtle multi-bands, especially in snow, would have been difficult to discern. Additionally based on only a few (14) of Novak et al.'s (2004) storms meeting our snow storm criteria, we surmise that many of the cool season storms were largely rain storms rather than snow storms. Novak et al. (2004) does not include information on the near surface temperatures or precipitation types.

Consistent with the results in Novak et al. (2004), storms exhibiting a band feature (single or multi-band) are more likely to be found in a mature cyclone compared a developing cyclone. Of the 63 mature cyclones in our study, 52 of them exhibited a band feature and 48 of them displayed multi-bands (Table 3.3). Snow storms with only multi-bands were twice as likely to be associated with a mature cyclone compared to a developing cyclone. Snow storms exhibiting coexisting single and multi-bands were over three times as likely to be associated with a mature cyclone compare to a developing cyclone (Table 3.3).

Non-banded storms were nearly twice as likely to be associated with a developing cyclone compared to a mature cyclone.

Most band features we observed developed and remained in the northwest quadrant of the cyclone; however, this result is strongly influenced by the position of the typical storm track relative to the radar domain along the NE US coast wherein the land (where the radars are located) is to the west of the low center track. Hobbs (1978) commonly found banding in the northeast quadrant of the cyclone based on coastal radar data in the Pacific Northwest, a situation where the radar was usually to the east of the low. In our data set, some multi-bands appeared to develop in the northeast quadrant and propagate into the northwest quadrant. In a couple of occasions, multi-bands were found in the southwest and southeast quadrants (Table 3.4), but the sample size from both the southwest and southeast quadrants is low. Single bands, when they occurred, were always found in the northern part of the cyclone, and the majority of single bands were found in the northwest quadrant similarly to Novak (2004). A few single bands were long enough to extend into multiple quadrants. Occasionally, single bands were observed to stretch from the northeast quadrant, through the northwest quadrant and into the southwest quadrant.

3.3.1 Band and Stratiform Precipitation

The band area, stratiform area, and total precipitation area for the northwest and northeast quadrants of the cyclone for each storm were compared for times of only snow. Mixed precipitations times were determined subjectively and excluded. The southwest and southeast quadrants were excluded due to precipitation infrequently observed in these quadrants. The preferred low track is over the ocean and the precipitation in southwest and southeast quadrants typically remains outside the range of our radar domain. Figure 3.1 illustrates how much of the total precipitation area in the northwest and northeast quadrants was classified as ether a band or stratiform by the convsf algorithm for each snow storm. Within the northwest and northeast quadrants, the proportion of the precipitation area within bands was on average ~7%. The storm duration maximum band area was ~24% and occurred during the February 5, 2001 storm.

The relative timelines between band and stratiform precipitation in these snow storms differs from the relationship between convective and stratiform precipitation a typical mesoscale convective system (MCS). In these snow storms, the stratiform precipitation tends to form first (Figure 3.2). In a typical MCS, convective precipitation, that is precipitation that is created by strong updrafts, forms prior to stratiform precipitation (Houze and Hobbs 1982). Stratiform precipitation in context of MCS is sometimes termed "old convection" and the area of stratiform significantly increases as the convective precipitation starts to weaken (Houze 1997). In these snow storms, however, stratiform precipitation forms prior to band precipitation implying a physical property that modifies the precipitation field after it is initially formed.

At any given location, storm total precipitation accumulation (A) is a function of both intensity (I) and duration (D) of precipitation. A simplified way to look at this is to assume that there are only two snow rates, one associated with bands and one associated with the stratiform precipitation. In this simple framework, the storm total accumulation could be estimated as:

$$A = I_b D_b + I_s D_s$$

where I_b is the snowfall intensity in bands, D_b is the duration of band precipitation, I_s is the snowfall rate in stratiform and D_s is the duration of stratiform precipitation. If band snowfall rates are X times larger than stratiform snow rates, it would take X minutes of stratiform precipitation to equal 1 minute of band precipitation. For a given location, depending on how long bands are present over the location and the relative intensity of the band snow rate relative to the stratiform snow rates, the percent of snowfall from the bands will vary. Based on vertically pointing radar data obtained at Stony Brook, typically snow bands are overhead less than 15 minutes at a time (perpendicular motion to the location), but their intensity is much stronger than the background stratiform precipitation yielding increased snow accumulations (Hoban et al. 2015). In this study, bands were said to move in one of two directions relative to the cyclone location: parallel and perpendicular. For example, for a snow band stretching along a line southwest to northeast, parallel motion would be to the northeast and perpendicular motion would be to northwest. These definitions are simplified

from Kenyon (2013) who split band motions into 4 categories. Perpendicular motion will result in shorter band durations over a given location where parallel movement results in the full length of the band training over a given location. Perpendicular motion of snow bands was more common (73% of bands) than parallel motion (27%). The relationship between band intensity and duration and the background stratiform intensity and duration will be examined further in future work.

3.4 General Wave Characteristics

Examination of the time-varying Doppler velocity fields yielded detection of wave-like features in 54 out of the 108 storms (50% of storms) (Table 3.5). Velocity waves were usually observed for only a subset of storm duration and in a portion of the precipitation area. Velocity waves were detected moving into the precipitating portion of the storm within the radar domain from along either the south or southeast boundary of the precipitation area. We did not observe velocity waves originating in the middle of a precipitation area. Based on their locations and motions, the velocity waves appear to originate in the vicinity of the low center or to south of the low in an area that was either usually outside our multi-radar coverage and/or did not have precipitation echo. An important caveat in our radar-based analysis is that we can only observe Doppler velocity where there is precipitation. Velocity waves could be present in the dry slot or in areas with clouds, but no precipitation, we would not be able to observe them.

In the 54 snow storms observed to exhibit waves, 96% of the storms had waves in the northwest quadrant and 57% had waves in the northeast quadrant. Many waves were seen to first appear in the northeast quadrant and then propagate into the northwest quadrant. This movement of the waves is consistent with overall circulation around the low. In a Lagrangian framework centered on the low, waves were seen to rotate counterclockwise around the cyclone center in the same general direction as the clouds and precipitation (neus perusal page: precip.meas.ncsu.edu/neus/perusal).

Table 3.5 summarizes the number of storms with and without waves present. There is no difference in the number of storms with waves (54) and the number of storms without

waves (54). Of the storms with waves, the majority of the waves (66%) were found during the mature stage of the cyclone. Waves were twice as likely to be found in a storm with a mature cyclone compared to a storm with a developing cyclone. Storms without waves were found to be associated with nearly equal numbers of mature and developing cyclones. As mentioned previously, only a few storms are suitably located relative to the radar domain to obtain samples of precipitation within the southeast and southwest quadrants of the cyclone, so the remainder of the discussion on velocity waves and their relation to bands focusses on the northwest and northeast quadrants. The association between velocity waves and different types of bands is described in Table 3.3. Only 4 of the 54 storms with waves did not contain multi-bands. One storm was single band only, 25 were multi-band, 25 have coexisting single and multi-bands, and 3 were non-banded.

We originally hypothesized that multi-bands would be associated with localized convergence at the band in a manner similar to the convective circulation tied to generating cells (Rosenow et al. 2014) and as previously observed in single bands (Novak et al. 2008). However, we found no consistent, sustained convergence signatures in the Doppler radial velocity data associated with multi-bands. It is possible that the convergence is either episodic or could occur as an initial pulse that creates the snow band. Once a snow band forms, it takes approximately an hour for the locally enhanced snow to fall 4 km (based on a fall speed of 1 m/s). Based on the radar observations, waves are not required for multi-bands to occur but velocity waves and snow bands do frequently occur together.

Figure 3.3 is a simple schematic of the interaction between multi-bands and Doppler velocity waves. The concurrence between multi-bands and waves could yield several potential outcomes. The first is that waves and multi-bands coexist, but there is no interaction between them. The second is that waves have a balanced interaction with multi-bands meaning that the impact of upward (Figure 3.3b) and downward motions (Figure 3.3c) essentially cancels out so there is no net enhancement of the multi-band. The third option is that waves have an unbalanced interaction with multi-bands yielding net enhancement and/or formation of the multi-bands from the upward motion associated with the waves (Figure

3.3b). Technically, the downward motion associated with waves (Figure 3.3c) could act to disperse the multi-bands, but we do not observe that.

We took a vertical cross section through reflectivity data, radial velocity data, Doppler velocity waves data, and instantaneous radial convergence/divergence data in an attempt to understand their interaction (Figure 3.4, Animation 3.4). We are limited by the coarse vertical resolution of the WSR-88D radar scan. One can follow the snow band in reflectivity as it moves toward the radar. The detection of the Doppler velocity waves and instantaneous convergence/divergence is less continuous and it is harder to follow. Overall, it is difficult to make any conclusions regarding the interactions between the snow bands and the waves using these vertical cross-sections from the WSR-88D radar. The 12 Feb 2006 example represents one of the few times that the snow bands and Doppler velocity waves moved along a radial of the radar.

At this time, we do not have solid evidence to indicate how the multi-bands and waves interact, but we will discuss a few potential types of interactions. The upward motion associated with the wave could simply retard the falling of the snow, increasing the residence time of the particles in the band, and yielding a longer lasting multi-bands. The downward motion may balance the effects of the upward motion and increase the downward speed of snow particles. Snow does not fall like small rain drops where the actual fall speed is the sum of the vertical air motion and particle fall speed when w=0 m/s. Rather, snow tends to swirl. The interaction of a swirling snow particle with the upward and downward air motions is not addressed in the literature. It may be that the impact of upward and downward vertical air motions applied to swirling particles are not balanced. Experimentation is needed to resolve this.

The convergent motion may bring together smaller snowflakes forming an area with a high number concentration of snow particles. Figure 3.5 shows a high concentration of snow particles associated with band passage on 27 Jan 2015. The Multi-Angle Snowflake Camera image shows hundreds of flakes in a volume the size of a baseball. However, this localized convergence of flakes would be reversible in divergent flow.

Localized upward motion within the wave may also increase vapor deposition leading to growth of snow particles. Vapor deposition also yields latent heating leading to more buoyancy and increased upward motion within the snow band. Downward motion within the interior of the cloud would likely not cause either evaporation or sublimation. Separating among these potential effects will likely require field project data sets obtained from aircraft.

We also examined the relationships of waves and the direction of movement of the bands. For example, for a snow band stretching along a line southwest to northeast, parallel motion would be to the northeast and perpendicular motion would be to northwest. Perpendicular motion of snow bands was more common (Table 3.6). For snow storms with coexisting single and multi-bands 19 out of the 25 snow storms with waves had perpendicular band movement and were associated with waves. For multi-band only snow storms, 19 out of the 31 snow storms had perpendicular band movement and waves. Parallel band movement occurred in about the same number of storms with and without waves. Kenyon (2013) went a step further to divided band motion into 4 categories and examined the environmental factors related to each category of band motion. Kenyon (2013) found a key component of band motion was its location relative to the cyclone. It would be interesting to expand upon this work in the future work and examine how waves move in different regions of the cyclone.

We examine the joint characteristics of band area relative to precipitation area and stratiform fraction, whether velocity waves are present or not, and the type of band in Figure 3.6 and Figure 3.7. In the NW quadrant, storms with larger band areas nearly always have coexisting single and multi-bands and typically had velocity waves present (Figure 3.6). In contrast in the NE quadrant, larger band areas within a storm could be obtained with either coexisting single and multi-bands or just multi-banded conditions (Figure 3.6). As in the northwest quadrant, storms with higher band area in the northeast quadrant typically had velocity waves present. Figures 3.6 and 3.7 compare the storm total precipitation area and the percent of precipitation that is stratiform. The majority of storms had stratiform precipitation making up over 92% of the total precipitation area. Storms where stratiform precipitation made up less than 92% of the total precipitation were nearly all either coexisting

single and multi-bands or just multi-banded and typically had waves present. Note that for 16 storms without trackable lows, the quadrants where the precipitation is present are not defined and these storms are not included in the Figures 3.6 and 3.7. The only single-band snow storm with waves in our data set did not have a well-defined low.

Multiple elevation angles from radar data are used to estimate the vertical extent of Doppler velocity waves. Waves were found in the nearly same location through multiple radar tilts indicating that the velocity wave features were nearly vertical. If waves were present, they were always found to exist in the lowest tilt, and waves were never found to exist in a higher radar elevation angle without being found in the lowest tilt first. Figure 3.8 illustrates the range of depths waves were present. Based on the radar data available, average depth for the storms examined was 4 km with a maximum depth a 9.5 km and a minimum depth a 1.75 km. Wavelength was estimated using the data in lowest tilt. Figure 3.9 illustrates the range of wavelengths found for velocity waves. The average wavelength was 15 km and waves demonstrated a range of 10-30 km.

3.5 Band and Wave Speeds

Snow band and Doppler velocity wave speed and direction were calculated over 1° latitude x 2° longitude boxes using the method described in Section 2.10. Snow bands and waves were described as "related" if their direction of motion were within 25° of each other. Of the 54 storms with waves and bands, 46 had velocity wave motion within 25° of the motion of the concurrent snow bands. For each of the 54 storms with velocity waves, one 1° x 2° box was used. The location of the box was determined subjectively to be the area of the most clearly defined waves associated with snow bands.

Figure 3.10 illustrates the speeds for both snow rate and waves. Based on the radar data examined within the boxes, the average snow band speed is 16.5 m/s while the average velocity wave speed is 21 m/s. The difference between the snow band speed and the velocity wave speed for each of the 46 storms were the motions were within 25° (Figure 3.10c) indicates that the velocity waves generally moved faster than the snow bands. Waves were found to move faster than snow rate in 41 snow storms and snow rate was found to move

faster than waves in 5 storms. The difference in wave and snow rate speed suggests that the velocity waves are not locked to the snow bands.

3.6 Wave Mechanism

Wind directions from radar-derived VAD profiles at KOKX were compared to the movement direction of waves and of snow bands. The snow storms in our data sets are typically associated with a lot of shear and it was not uncommon to find a layer of winds within the VAD profile moving in the same direction as the waves somewhere over the depth of the waves. The height of the layer with matching directions varied and sometimes did and sometimes did not correspond to the stable layer. Due to the large amount of shear associated with these snow storms, the movement of the waves was compared to the mean flow in two separate layers from the VADS: the surface layer (0-2 km) and the above surface layer (2-4km). The majority of occurrences of velocity waves (46 out of 54) moved in a direction more than 45° different than the wind direction in the near surface layer (0-2 km). However, nearly the opposite was found for the above surface layer (2-4 km) with the majority (39 out of 54) of waves moving similarly (within 45°) to the mean flow. It is unclear whether or not either layer affects the movement of the velocity waves. Waves moving in a direction different than the mean flow is a key characteristic of gravity waves and we hypothesize that most of the time the velocity waves we are observing are gravity waves. Gravity waves need a stable layer to travel though (i.e. a wave duct) (Lindzen and Tung 1976). Based on the accepted schematics of cyclones (Ahrens and Henson 2016), stable layers are present behind the cold front, in front of the warm front, and associated with the occlusion. A stable layer can occur in the dry slot area behind the cold front where there is no precipitation. In many storms, we infer that the waves are propagating through the dry slot before reaching the precipitation area in the NW quadrant of the storm. A confounding feature of the velocity waves is their large vertical extent which is often deeper than the stable layers present in the upper air data. A more complete analysis of the relationship between wave ducting and the velocity waves is left for future work.

Doppler velocity waves always appeared along the edge of the precipitation echo rather than inside it implying that the waves formed where we cannot observe them with the operational radar network. Since we cannot observe where the waves form, the potential triggering mechanism is highly uncertain. We hypothesize that the trigger mechanism could be related to latent heat release in convection along the cold front or the warm front. Another potential wave trigger could be geostrophic adjustment associated the jet streak (Allen et al 2012). It is possible that not all Doppler velocity waves were triggered by the same mechanisms and multiple mechanisms or other mechanisms not discussed here could contribute to the formation of the Doppler velocity waves. These ideas will be further examined in future work.

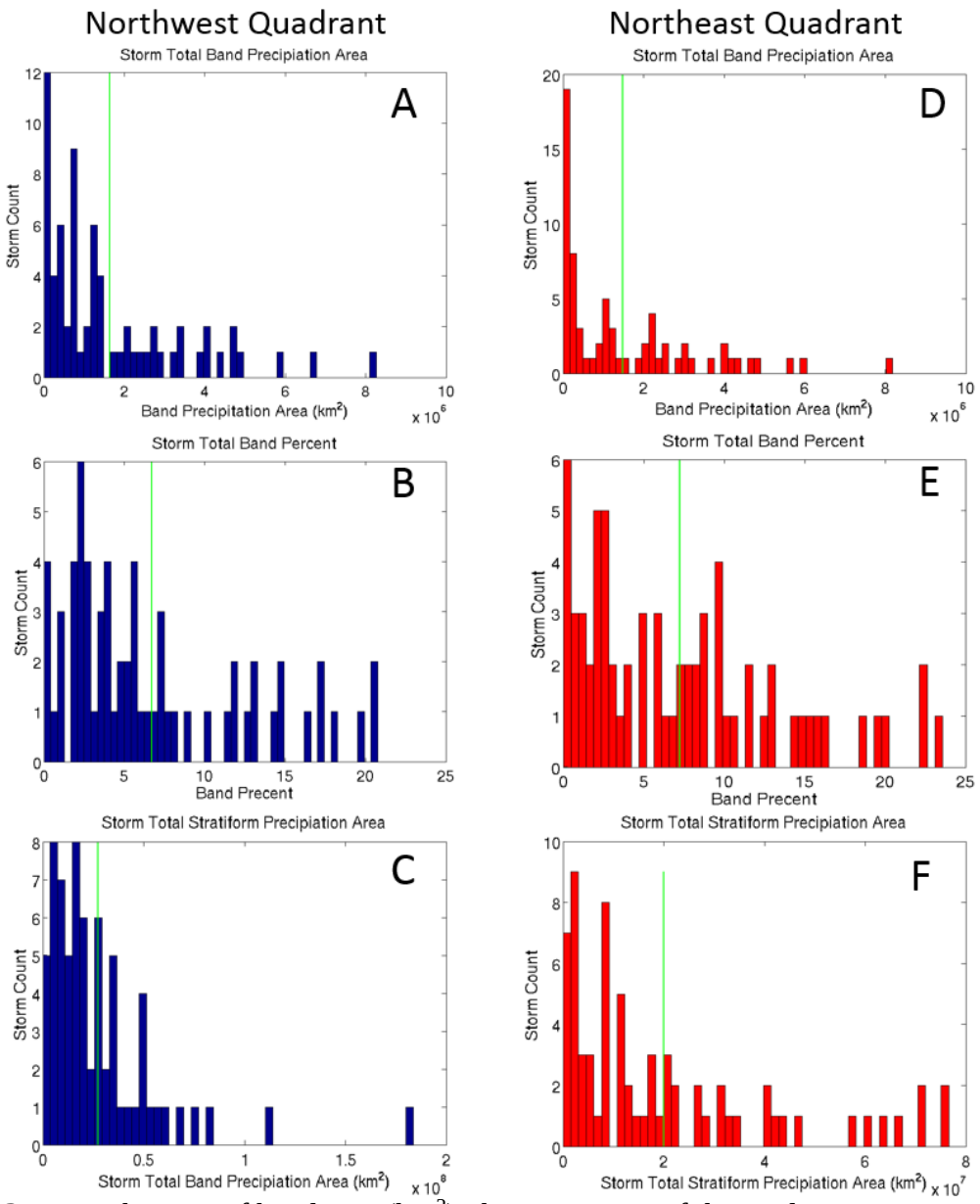

Figure 3.1 Distributions of band area (km^2), the percentage of the total precipitation area that is classified as bands, and stratiform area (km^2) summed over individual storm durations for the northwest and northeast quadrants. (A) Storm total band precipitation area for the northwest and the (D) northeast quadrants. (B) The band percentage of the storm total precipitation area for the northwest and the (E) northeast. (C) The storm total stratiform precipitation area for the northwest and (F) northeast Green lines represent the mean value for each plot.

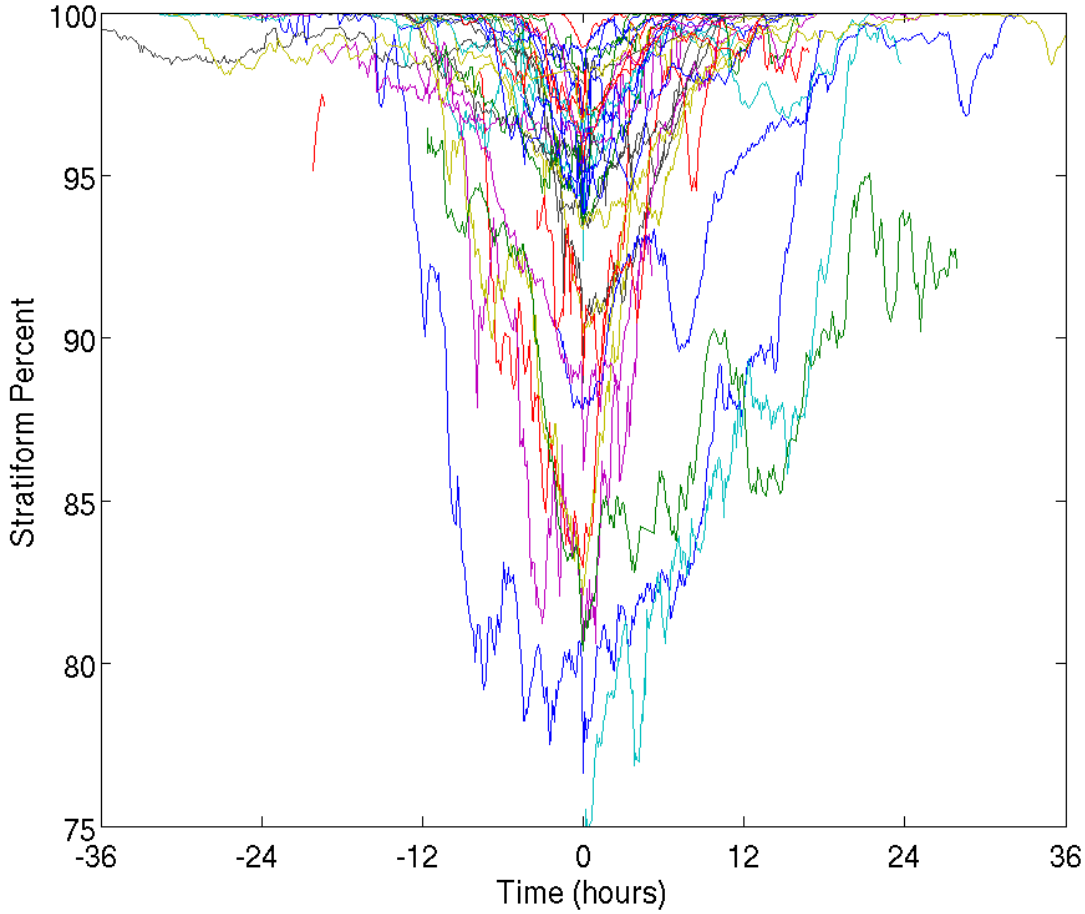

Figure 3.2 Time series of percent of total precipitation that is stratiform for storms containing only snow (34 storms). The time series are adjusted so that time=0 corresponds to time of the minimum percent of stratiform precipitation.

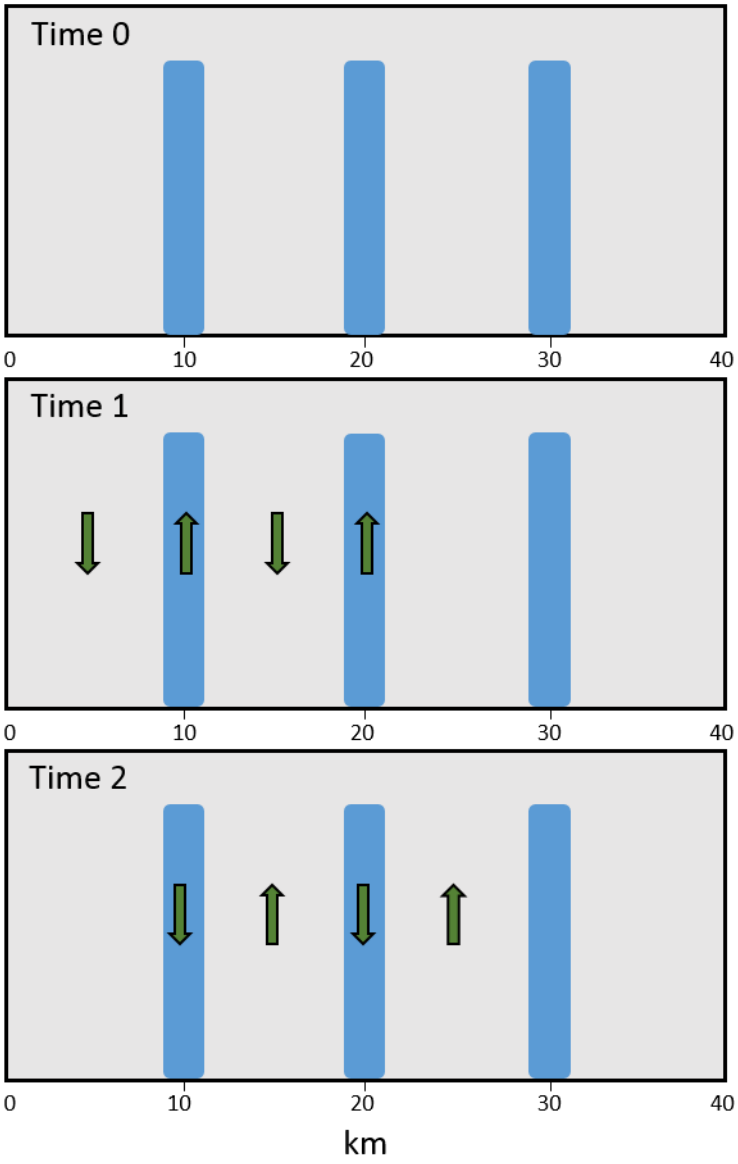

Figure 3.3 Time 0 represents a simple schematic of multi-bands (blue shading) prior to any interaction with waves (green arrows). Time 1 indicates the upward motion (up arrows) associated with waves interacting with multi-bands. Time 2 is 4 minutes later (based on an averaged Doppler velocity wave speed of 21 m/s) indicates the downward motion (down arrows) interaction with the multi-bands.

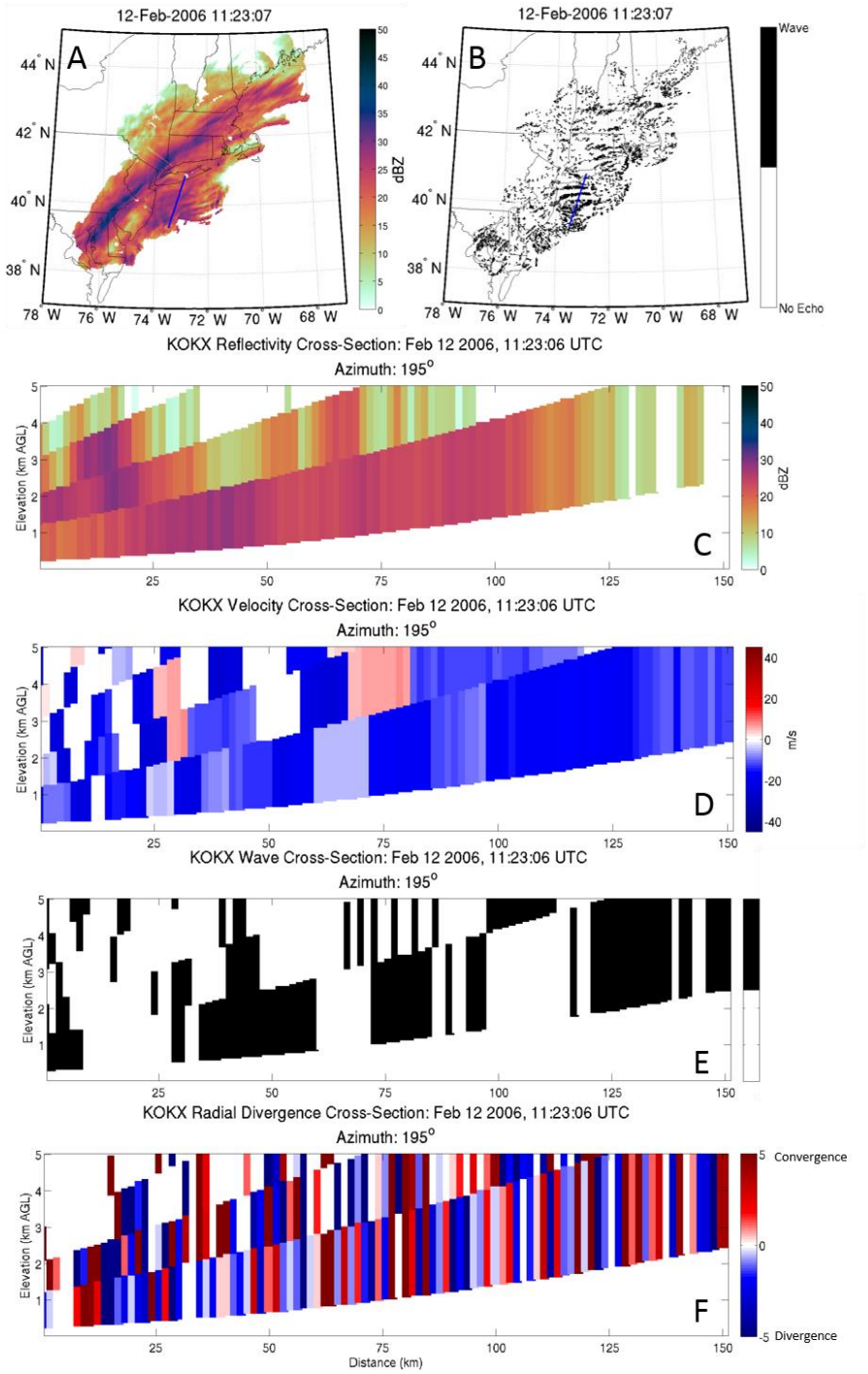

Figure 3.4. Stitched regional maps A) of reflectivity for February 12, 2006, 11:28:57 UTC and B) of the Doppler velocity waves data. C) Vertical cross-sections taken through azimuth 195° (indicated by the blue line in A) and B)), C) of reflectivity, D) of radial velocity, E) of the Doppler velocity waves data and F) of instantaneous radial convergence/divergence.

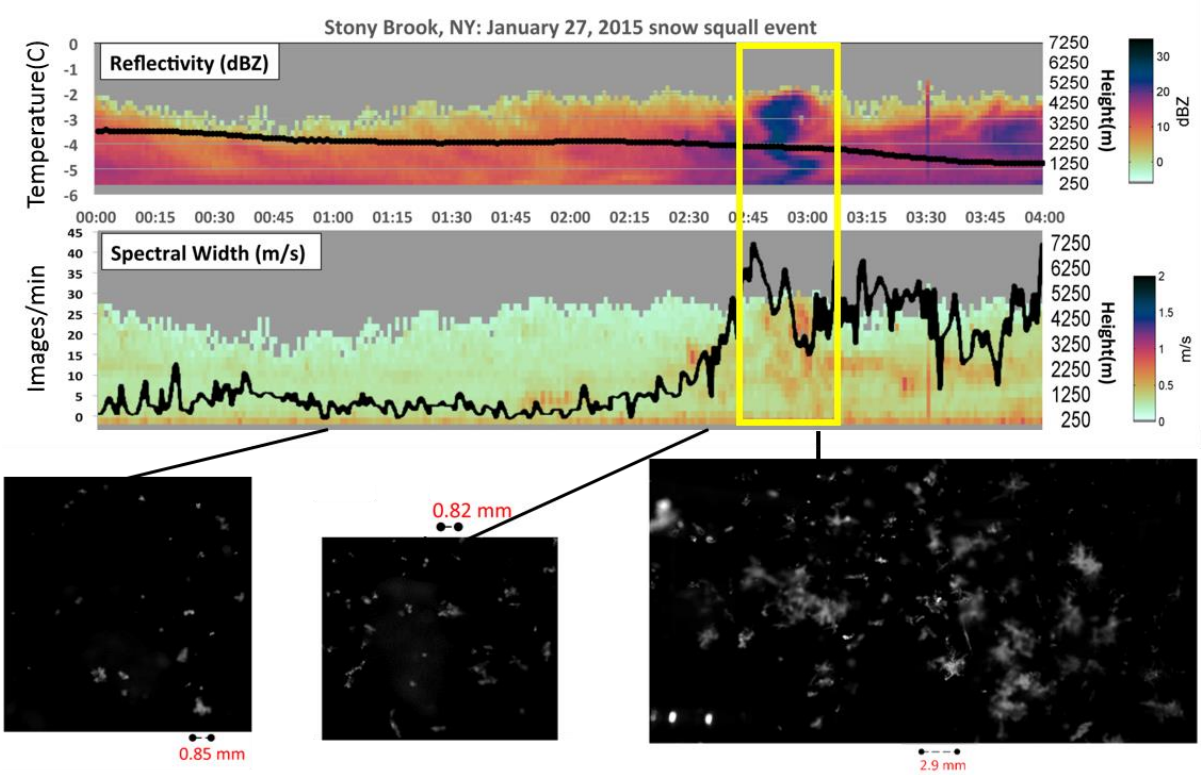

Figure 3.5. Reflectivity (top) and Spectral Width (middle) from a Micro-Rain-Radar (MRR) for January 27, 2015. The black line overlaid on Reflectivity represents the surface air temperature. The black line overlaid on Spectral Width represents the number of times per minute the Multi-Angle Snow Camera (MASC) was trigger. The images at the bottom were taken by the MASC at various times throughout the snow storm. The yellow box indicates the time of the band passage.

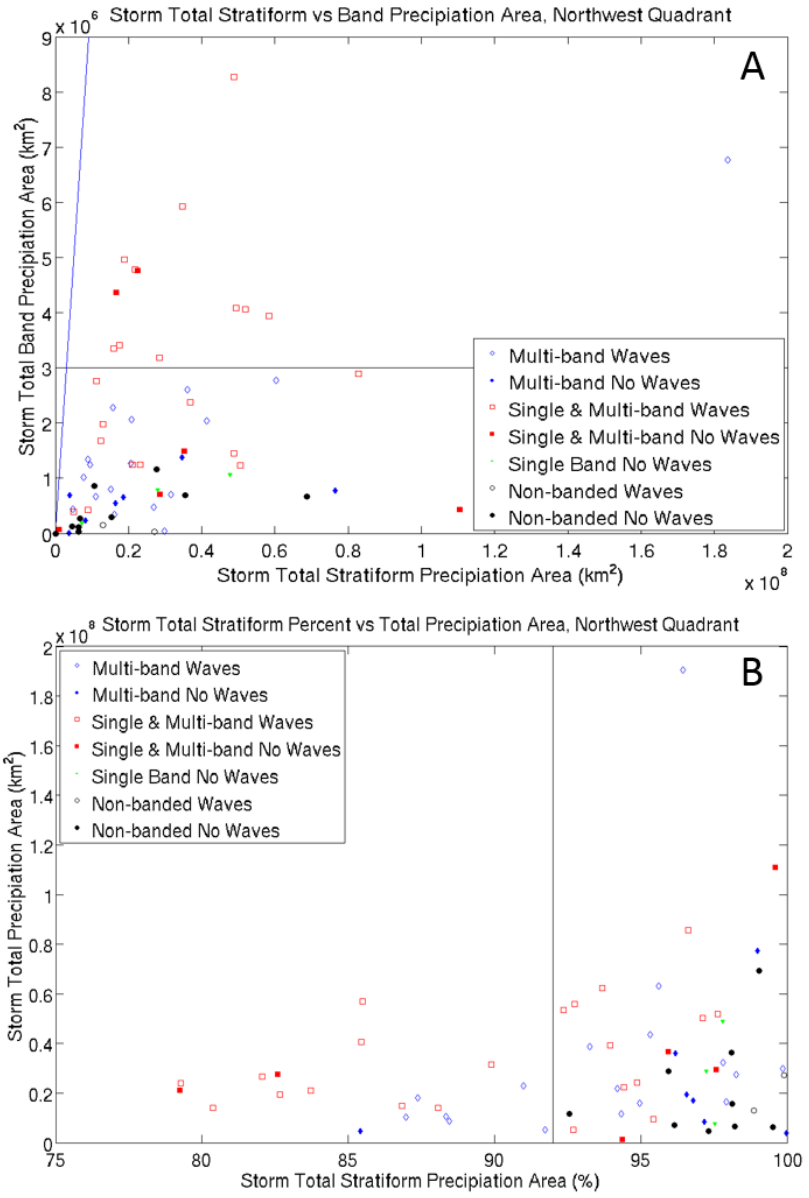

Figure 3.6 Storm total precipitation area characteristics categorized by the storm's band type and whether waves were present for the northwest quadrant. A) Storm total stratiform precipitation area compared to storm total band area. The blue line represents the one to one line of storm total stratiform area and storm total band area. The black line is 3 x 10^6 km^2. B) Percent of stratiform area compared to the storm total precipitation area. The black line is 92%.

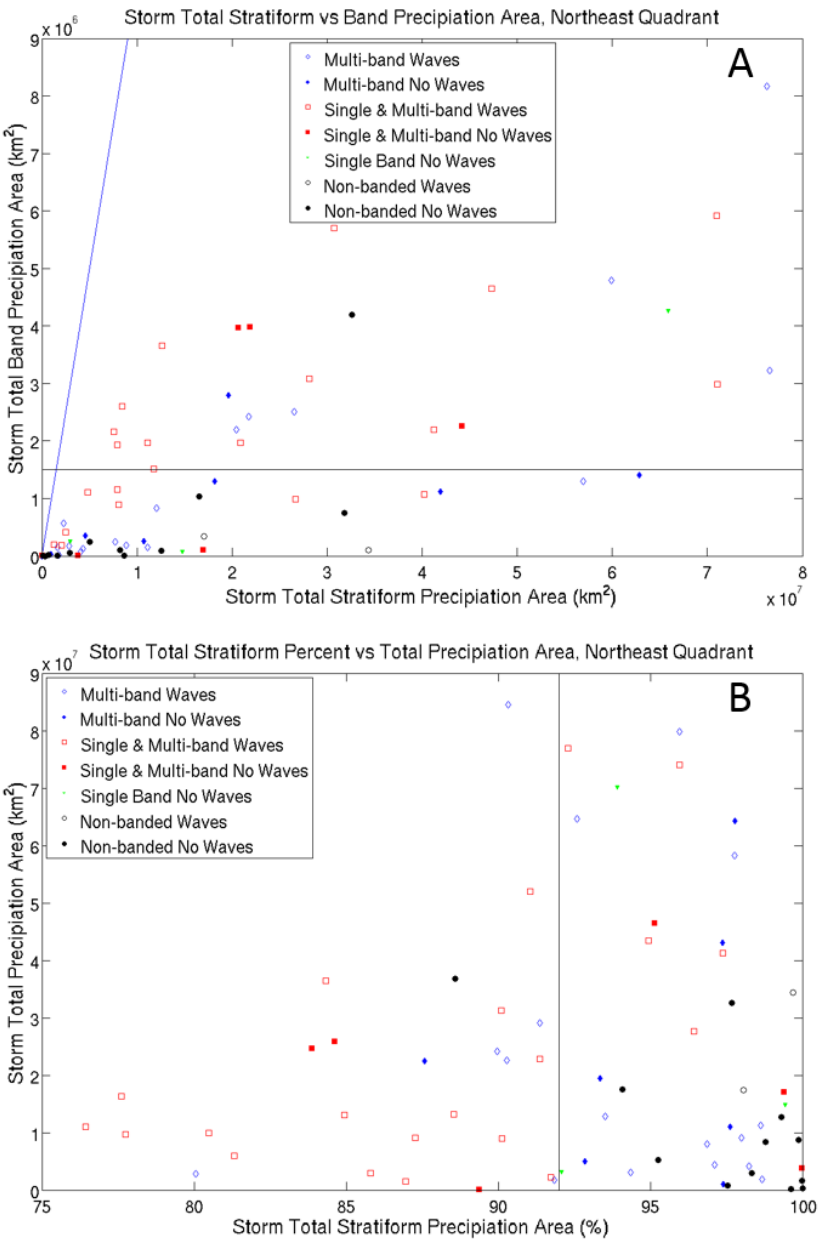

Figure 3.7 As in figure 3.3, but for the northeast quadrant. The black line in A) is 1.7 x 10^6 km^2.

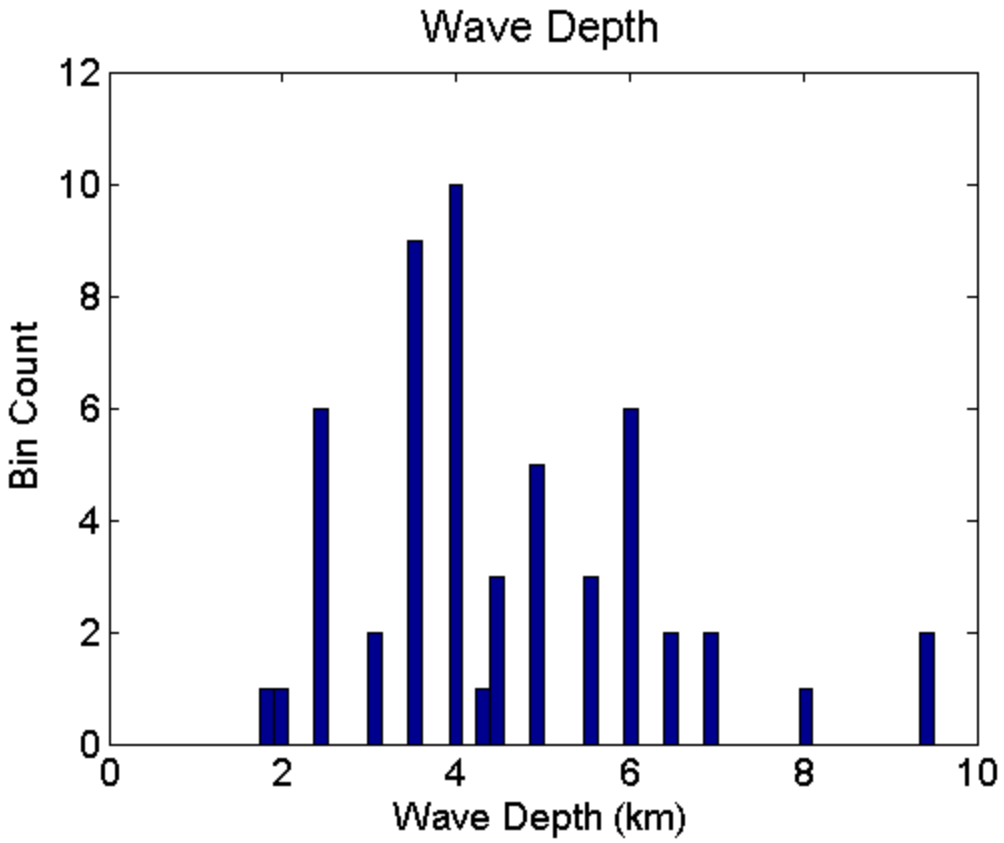

Figure 3.8 Histogram of average wave depth for the each of the 54 snow storms where waves were observed.

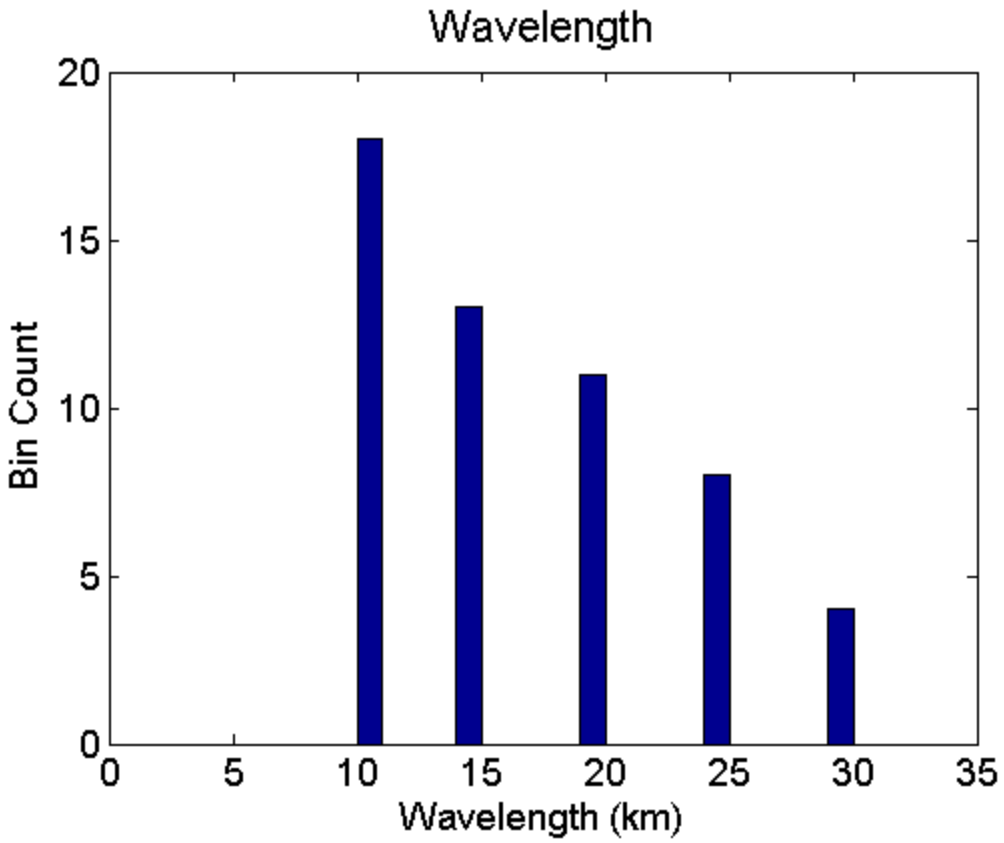

Figure 3.9 Histogram of the ranges of wavelengths estimated in Doppler velocity waves based on data from 54 storms with waves.

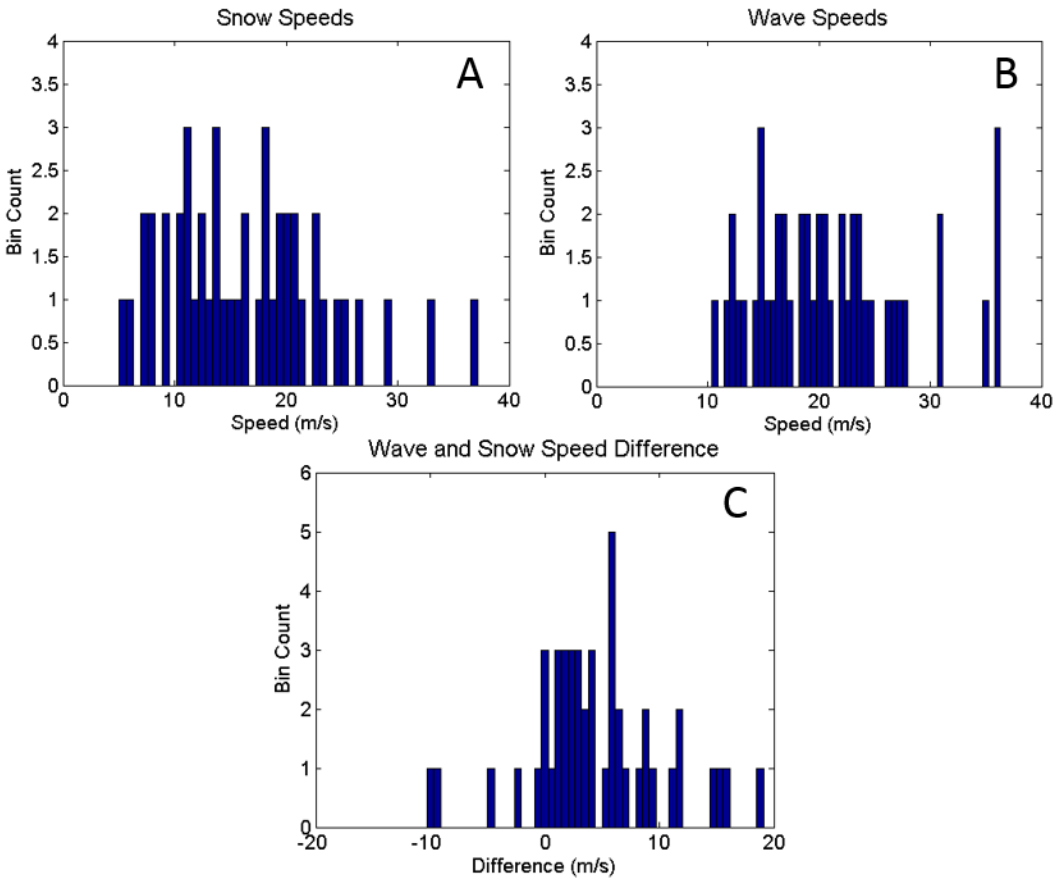

Figure 3.10 Distributions of snow band and velocity wave speeds based on 1° x 2° boxes in the 51 snow storms with both bands and waves. (A) Distribution of snow band speeds. (B) Distribution of velocity wave speeds. (C) Distribution of speed difference between snow bands and velocity waves when their direction of motion differed by less than 45°. A positive value indicates velocity waves moving faster than snow bands.

Table 3.1 Synoptic characteristics while the storm was within the radar domain for the 108 snow storms. A given storm could have either a simple or complex front configuration and be in either a developing stage, mature stage or not associated with a strong low center. A given storm could have both a cold front and a warm front. The thick black lines represent where totals could equal 108 if the synoptic characteristics was found in each storm.

Synoptic characteristics	**Number of Storms**
Simple front configuration	68
Complex front configuration	40
Mature stage with occluded front	63
Developing stage	31
No strong low center	14
Cold Fronts	103
Warm Fronts	98

Table 3.2 Information on cyclone track a) direction and b) location for each of the 108storms. The category “too weak” indicates a low center that was sufficiently weak and diffuse to not yield a usable track based on the NARR model output.

A. Track Direction	Number of Storms
Northeast	77
East	15
Southeast	2
Too Weak	14

B. Track Location	Number of Storms
Ocean	63
Ocean to Land	2
Land	6
Land to Ocean	23
Too Weak	14

Table 3.3 The number of storms for each band classification with velocity waves and in mature or developing stages. A given storm could be in either a developing or mature stage.

	Total Number of Storms	**Number of storms with Waves**	**Number of Mature Storms**	**Number of Developing Storms**
Single Band	7	1	4	3
Multi-Band	39	25	23	16
Single and Multi-Band	32	25	25	7
Non-banded	30	3	11	19
Total	108	54	63	45

Table 3.4 The number of snow storms with band features and with waves found in each quadrant broken down by band classification.

Quadrant	**NW**		**NE**		**SW**		**SE**	
Feature Type	Band	Waves	Band	Waves	Band	Waves	Band	Waves
Single Band	5	1	4	1	2	0	0	0
Multi-Band	31	25	27	11	6	4	1	0
Single and Multi-band	32	24	26	19	10	3	0	0
Non-banded	0	1	0	3	0	0	0	0

Table 3.5 The number of storms with and without waves that are associated with mature cyclones and developing cyclones.

	Number of Storms with Waves	**Number of Storms without Waves**
Total number of storms with Waves	54	54
Mature	36	27
Developing	18	27

Table 3.6 The total number of storms with and without waves, snow storms with perpendicular band movement with and without waves, and snow storms with parallel movement with and without waves.

	Number of Storms with Waves	**Number of Storms without waves**	**Waves & Parallel**	**Waves & Perpendicular**	**No Waves & Parallel**	**No Waves & Perpendicular**
Multi-Band	25	14	6	19	3	11
Single and Multi-Band	25	7	5	20	2	5
Single Band	1	6	1	0	4	2
Non-Banded	3	27	NA	NA	NA	NA

CHAPTER 4 – Conclusions

This study combines radar data from 6 NWS operational radars to characterize the spatial distribution and variability of precipitation and velocity features from 108 snow storms in the northeast United States along the corridor from Dover, DE to Portland, ME. While snowfall accumulation varies geographically storm to storm (e.g. Gaffin etl al. 2002; Novak et al. 2004; Colle and Yuter 2007; Novak et al. 2008; Stark et al. 2013; Picca et al. 2014) over the entire 108 storm data set there is no strong localized enhancement in estimated snow rate associated with geographic features such as coastlines or low hills. This lack of localized snow enhancement is likely related to the wide variability in wind direction at any given location as extratropical cyclones with diverse tracks traverse the region.

Storms were classified based on the geometry and number of snow bands present throughout their observed life cycle following the classification schemes of Ganetis et al. 2015. Storms exhibiting one or more band features were more frequently observed to be associated with a mature cyclone compared to a developing cyclone. This may be due to the airstreams in the mature cyclone being further developed. For example, the warm conveyor belt splits and brings essential moisture and potentially destabilizing air to the northwest quadrant of the cyclone. Storms with solely multi-bands were the most common, representing 36% of snow storms. Storms with coexisting single and multi-bands occurred in 30% of the events and storms without any clearly defined snow bands represented 27% of events. Snow storms manifesting only a single band were the least common occurring in only 7% of snow storms. Novak et al. 2004 examined 88 snow, mixed precipitation, and rain events during the October-April cool seasons and found single bands to be most common. Only 14 of the Novak et al. (2004) events met our 1” of snow storm criteria. Most band features were observed to develop and remain in the northern part of the cyclone with all single bands having the majority of their length in the northwest quadrant and multi-bands were primarily found in the northeast and northwest quadrant. These results are greatly influenced by the location of our radar domain and the observed cyclones tracks where the land (location of the radars) is typical located to the north or northwest of the cyclone.

The relative timelines between band and stratiform precipitation in these snow storms differs from the relationship between convective and stratiform precipitation in a typical mesoscale convective system. In a typical deep convective system, stratiform precipitation develops from aging convective precipitation. In these snow storms, stratiform precipitation forms *prior* to band precipitation. This sequence implies a physical process for band formation that locally enhances precipitation within the stratiform precipitation.

On average, storm total band area only represented ~7% of the total precipitation area and the maximum storm total band observed was 24%. Bands by definition represent large gradients within snowfall rates. Over the same number of hours of precipitation, fast moving bands will increase average accumulation compared to when no bands are present. Bands would have the most impact on accumulation when their higher intensity snowfall is present for prolonged periods of time. Bands can linger over a given location if storm motion and storm rotation are slow or if a segment of a single band acts as a pivot point for rotation of the band itself. Multiple bands could also sequentially pass over a given location in a similar manner to how training cells are responsible for flooding. The low proportion of band area to total precipitation area suggests that the role of bands in snowfall accumulation is strongly modulated by their speed of motion. Distinguishing among storms with more stationary versus faster moving bands may be a relevant forecast problem.

Previous research has shown that single bands are associated with sustained (multiple hours) areas of frontogenesis (Novak et al. 2004; Novak et al. 2008; Novak et al 2010; Stark et al. 2013). The mechanisms controlling the initiation and lifecycle of multi-bands remain uncertain. A typical snow particle falling at ~ 1 m/s takes a little more than an hour to fall 4 km. Hence upward motion conditions favorable for formation of snow bands could be short-lived compared to duration of the snow band itself.

In looking at radial velocity data, we often noticed transient features that moved perpendicular to the mean flow. We developed a method to isolate these features from the radial velocity data and found that they were consistent across the adjacent radar domains. We referred to these features as Doppler velocity waves. Our hypothesis is that Doppler velocity waves contribute to multiband formation and maintenance. Seventy percent of

occurrences of multi-bands (with or without coexisting single bands) are associated with velocity waves and the similar orientations of the velocity waves and snow bands suggests a connection between the two. Waves were found to generally move faster (average of 4.5 m/s faster) than snow bands suggesting that velocity waves were not locked to snow bands in the same way that overturning circulations are locked to snow generating cells (Rosenow et al. 2014). Velocity waves do not need to move in step with localized snow bands to cause or enhance snow bands. A wave could trigger a snow band and then move away from it. Additionally, after initial formation, a snow band could briefly coincide with the upward motion from a subsequent wave enhancing and maintaining the existing band in a manner similar to the interaction of gravity waves with discrete propagation of squall lines proposed by Fovell et al. (2006).

Doppler velocity waves were found to move differently than near surface layer (0-2 km) in 46 out of 54 (85%) snow storms. However, nearly the opposite was found for the above surface layer (2-4 km) with the majority (39 out of 54) of waves moving similarly (within 45°) to the mean flow. It is unclear whether or not either layer affects the movement of the velocity waves. Waves moving in a direction different than the mean flow is a key characteristic of gravity waves and we hypothesize that most of the time the velocity waves we are observing are gravity waves. Gravity waves need a stable layer (a wave duct) to travel through (Lindzen and Tung 1976) and extratropical cyclones have stable layers present behind the cold front, in front of the warm front, associated with the occlusion and potentially in the dry slot. Doppler velocity waves always appeared along the edge of the precipitations echo rather than inside it implying that waves formed where we cannot observe them with the operation radar.

When forecasting snow accumulation, both the presence of bands and the amount of time a band spends over a given location is key. No clear, sustained convergence signals were observed with multi-bands suggesting they are not the product of generating convective cells. The relationship between multi-bands and Doppler velocity waves remains unclear. Doppler velocity waves are not required for the formation of multi-bands, but they are typically found together suggesting a relationship between waves and multi-bands.

A field project is needed to obtain aircraft in situ and remote sensing data sets including cloud radar, cloud lidar, and dropsondes that can address many of the unresolved issues raised by this study. Key questions that will require detailed research observations to resolve are: whether and how waves may be relevant for localized snow enhancement in bands, the trigger mechanisms behind the Doppler velocity waves, and the relationship between wave ducting and the velocity waves.

REFERENCES

Ahrens, C. D. and R. Henson 2016 Ahrens, C. D. (2016). Meteorology Today. (J. Warde, Ed.) (11th ed.). Brooks/Cole.

Allen, G., Vaughan, G., Toniazzo, T., Coe, H., Connolly, P., Yuter, S. E., and Ayers, J. K., 2012: Gravity-wave-induced perturbations in marine stratocumulus. Quarterly Journal of the Royal Meteorological Society, 139(670), 32–45. doi:10.1002/qj.1952

Churchill, D. D., and R. A. Houze Jr., 1984: Development and structure of winter monsoon cloud clusters on 10 December 1978. J. Atmos. Sci., 41, 933–960.

Clark, J. H. E., R. P. James, and R. H. Grumm, 2002: A reexamination of the mechanisms responsible for banded precipitation. Mon. Wea. Rev., 130, 3074– 3086, doi:10.1175/1520-0493(2002)1302.0.CO;2.

Colle, B. A., and S. E., Yuter, 2007: The Impact of Coastal Boundaries and Small Hills on the Precipitation Distribution Across Southern Connecticut and Long Island, NY. Mon. Wea. Rev, 135, 933-954.

Colle, B. A., D. Stark and S. E. Yuter, 2014: Surface microphysical observations within East Coast winter storms on Long Island, NY. *Mon. Wea. Rev.*,142, 3126-3146.

Corbin, N. A., 2016: Northern California's Central Valley Spatial Precipitation Patterns Associated with Atmospheric Reivers Under Different Environmental Conditions, M.S. Thesis, Dept. of Marine, Earth, Atmospheric Sciences, North Carolina State University, 227 pp.

Crum, T. D., and R. L. Alberty, 1993: The WSR-88D and the WSR-88D operational support facility.*Bull. Amer. Meteor. Soc.*, 74, 1669–1687, doi:10.1175/1520-0477(1993)074<1669:TWATWO>2.0.CO;2.

Cunningham, J., and S. Yuter, 2014: Instability Characteristics of Radar-Derived Mesoscale Organization Modes within Cool-Season Precipitation near Portland, Oregon*. Monthly Weather Review, 142, 1738–1757, doi:10.1175/MWR-D-13- 00133.1.

Davis, and K. A. Emanuel, 1991: Potential vorticity diagnostics of cyclogenesis. Mon. Wea. Rev., 119, 1929–1953, doi:10.1175/ 1520-0493(1991)119,1929:PVDOC.2.0.CO;2.

Emanuel, K. A., 1985: Frontal circulations in the presence of small moist symmetric stability. J. Atmos. Sci., 42, 1062–1071, doi:10.1175/1520-0469(1985)042,1062:FCITPO.2.0.CO;2

Fovell, R. G., Mullendore, G. L., & Kim, S. H. (2006). Discrete Propagation in Numerically Simulated Nocturnal Squall Lines. Monthly Weather Review, 134, 3735–3752

Gaffin, D. M., S. S. Parker, and P. D. Kirkwood, 2002: An unexpectedly heavy and complex snowfall event across the southern Appalachian region. *Wea. Forecasting*, 18, 224–235

Ganetis, S. A., B. A. Colle, N. P. Hoban, S. E. Yuter and N. A. Corbin, 2015: Simulations of Multi-bands in the Comma Head of Northeast U.S. Winter Storms. Abstracts, 16th Conference on Mesoscale Processes, 3-6 August 2015, Boston, MA.

Jonathan J. Helmus, Scott M. Collis. (2016) The Python ARM Radar Toolkit (Py-ART), a Library for Working with Weather Radar Data in the Python Programming Language. *Journal of Open Research Software* 4.

Hoban, N. P., S. E. Yuter, B. A. Colle, S. A. Ganetis, and N. A. Corbin, 2015: Observed Characteristics of Mesoscale Snow Bands in the Coastal Northeast U.S., *16th Conf. on Mesoscale Processes*. 3-6 August 2015, Boston, MA.

Hobbs, P. V., 1978: Organization and structure of clouds and precipitation on the mesoscale and microscale in cyclonic storms. Rev. Geophys. Space Physics, 16, 741-755.

Houze, R. A., P. V. Hobbs, K. R. Biswas, and W. M. Davis, 1976: Mesoscale Rainbands in Extratropical Cyclones, Mon. Wea. Rev., 104, 868-878.

Houze, R. A., Jr., and P.V. Hobbs, 1982: Organization and structure of precipitating cloud systems.*Advances in Geophysics,* Vol. 24, Academic Press, 225–315

Houze, R. A. Jr, 1993: Cloud Dynamics. Academic Press, 573 pp.

Houze, R. A., 1997: Stratiform precipitation in regions of convection: A meteorological paradox? Bull. Amer. Meteor. Soc., 78, 2179–2196.

Janowiak, J. E., Joyce, R. J., & Yarosh, Y. (2001). A real-time global half-hourly pixel resolution infrared dataset and its applications. Bulletin of the American Meteorological Society, 82(2), 205–217. doi:10.1175/1520-0477(2001)0822.3.CO;2

Kenyon, J. S., 2013: The Motion of Mesoscale Snowbands in Northeast U.S. Winter Storms, M.S. Thesis, Dept. of Atmospheric and Environmental Sciences, University of Albany, 122 pp.

Kocin, P. J., P. N. Schumacher, R. F. Morales Jr., and L. W. Uccellini, 1995: Overview of the 12–14 March 1993 superstorm. *Bull. Amer. Meteor. Soc.*, 76, 165–182, doi:10.1175/1520-0477(1995)0762.0.CO;2.

Lindzen, R. S., and K.-K. Tung, 1976: Banded convective activity and ducted gravity waves. *Mon. Wea. Rev.*, 104, 1602–1617, doi:10.1175/1520-0493(1976)104<1602:BCAADG>2.0.CO;2.

Mapes, B. E. (1993). Gregarious Tropical Convection. Journal of Atmospheric Chemistry, 50(13), 2026–2037.

Marks, F. D., and P. M. Austin, 1979: Effects of the New England coastal front on the distribution of precipitation. *Mon. Wea. Rev.*, 107, 53–67, doi:10.1175/1520-0493(1979)107<0053:EOTNEC>2.0.CO;2.

Mesinger, F., and Coauthors, 2006: North American Regional Reanalysis. Bull. Amer. Meteor. Soc., 87, 343– 360.

Morcrette, C. J. and K. A. Browning, 2006: Formation and release of symmetric instability following Delta-M adjustment. Quart. J. Roy. Meteor. Soc., 132, 1073–1089.

NCAR, 2012: Reorder. [http://www.eol.ucar.edu/rdp/home/reorder.html].

NOAA National Weather Service, Radar Operations Center (1991): NOAA Next Generation Radar (NEXRAD) Level II Base Data. NOAA National Centers for Environmental Information. doi:10.7289/V5W9574V [2016]

Novak, D. R., L. F. Bosart, D. Keyser, and J. S. Waldstreicher, 2004: An observational study of cold season–banded precipitation in northeast U.S. cyclones. Wea. Forecasting, 19, 993–1010.

Novak, D. R., B. A. Colle, S. E. Yuter, 2008: High-resolution observations and model simulations of the life cycle of an intense mesoscale snowband over the northeastern United States. Mon. Wea. Rev., 136, 1433–1456.

Novak D. R., B. A. Colle, and A Aiyyer, 2010: Climatology and composite analysis of mesoscale precipitation band formation in the comma head of mid-latitude cyclones., Mon. Wea. Rev. 138, 2354-2374.

Novak D.R., and B. A. Colle, 2012: Diagnosing snowband predictability using a multi-model ensemble system. Wea. Forecasting, 27, 565-585

Picca, J. C., D. M. Schultz, B. A. Colle, S. Ganetis, D. R. Novak, and M. J. Sienkiewicz, 2014: The value of dual-polarization radar in diagnosing the complex microphysical evolution of an intense snowband. Bull. Amer. Meteor. Soc., 95, 1825–1834, doi:10.1175/BAMS-D-13-00258.1.

Pizzamei, M., S. L. Gray, and K. A.Browning, 2005: Cloud-resolving model simulations of multiplybanded frontal clouds. Q. J. R. Meteorol. Soc., 131, 2617–2637.

Ralph, F. M., and Coauthors, 2005: Improving short-term (0–48 h) cool-season quantitative precipitation forecasting: Recommendations from a USWRP workshop. Bull. Amer. Meteor. Soc., 86, 1619– 1632.

Rasmussen, R, M. Dixon, S. Vasiloff, F. Hage, S. Knight, J. Vivekanandan, and M. Xu, 2003: Snow nowcasting using a real-time correlation of radar reflectivity with snow gauge accumulation. *J. Appl. Meteor.*, 42, 20-36.

Rosenow, A. A., D. M. Plummer, R. M. Rauber, G. M. McFarquahar, and B. F. Jewett, 2014: Vertical velocity and physical structure of generating cells and convection in the comma head region of continental winter cyclones. *J. Atmos. Sci.*, http://dx.doi.org/10.1175/JAS-D-13-0249.1

Sanders, F., and L. F. Bosart, 1985: Mesoscale structure in the megalopolitan snowstorm of 11–12 February 1983. Part I: Frontogenetical forcing and symmetric instability. J. Atmos. Sci., 42, 1050–1061.

Sanders, F., 1986: Frontogenesis and symmetric instability in a major New England snowstorm. Mon. Wea. Rev., 114, 1847– 1862.

Schultz, D. M. and Schumacher, P. N., 1999: The use and misuse of conditional symmetric instability. Mon. Wea. Rev., 127, 2709–2732.

Schultz, David M., and Geraint Vaughan, 2011: Occluded Fronts and the Occlusion Process: A Fresh Look at Conventional Wisdom. Bull. Amer. Meteor. Soc., 92, 443–466.

Stark, D., B.A. Colle, and S.E. Yuter 2013a: Observed microphysical evolution for two East coast winter storms and the associated snow bands. Mon. Wea. Rev., 141, 2037-2057.

Steiner, M., R. A. Houze, Jr., and S. E. Yuter, 1995: Climatological characterization of three-dimensional storm structure from operational radar and rain gauge data. J. Appl. Meteor., 34, 1978-2007.

Wexler, R., and D. Atlas, 1959: Precipitation generating cells. *J. Atmos. Sci.*, 16, 327–332, doi:10.1175/1520-0469(1959)016<0327:PGC>2.0.CO;2.

Yuter, S. E. and R. A. Houze, Jr., 1997: Measurements of Raindrop Size Distributions over the Pacific Warm Pool and Implications for Z-R Relations. J. Appl. Met., 36, 847-867.

Yuter, S. E, S. E., R. A. Houze, Jr., E. A. Smith, T. T. Wilheit, and E. Zipser, 2005: Physical Characterization of Tropical Oceanic Convection Observed in KWAJEX. J. Appl. Met., 44, 385-414.

Yuter, S. E., J. Payne, D. Stark, B. A. Colle, and J. Crouch, 2011: Observational sensitivity study of the temporal and spatial patterns of orographic precipitation for winter storms near Portland, Oregon. J. Hydrometeor, 12, 329-351.

Xu, Q., 1992: Formation and evolution of frontal rainbands and geostrophic potential vorticity anomalies. J. Atmos. Sci., 49, 629–648

APPENDICES

APPENDIX A

This appendix contains for the animations contained in the thesis. All animations can be found through the following link:
https://drive.google.com/drive/folders/0B87y7v1Q_k1DRk5jT29QNkJfVTg?usp=sharing

Animation 2.3a: A regional reflectivity map animation from 14:08 UTC on 26 December to 18:15 UTC on 27 December 2010.

Animation 2.3b: A regional snow rate map animation from 14:08 UTC on 26 December to 18:15 UTC on 27 December 2010.

Animation 2.3c: A regional convsf map animation from 14:08 UTC on 26 December to 18:15 UTC on 27 December 2010.

Animation 2.3d: A regional waves map animation from 14:08 UTC on 26 December to 18:15 UTC on 27 December 2010.

Animation 2.5: A radial velocity animation from 26 December 2010 from 22:00 UTC to 23:27 UTC (left). An animation of the negative portion of the temporal difference field from 26 December 2010 from 22:00 UTC to 23:27 UTC (right).

Animation 2.7a: A regional snow rate map animation in Lagrangian framework from 14:08 UTC on 26 December to 18:15 UTC on 27 December 2010.

Animation 2.7b: A merged infrared animation in Lagrangian framework from 14:00 UTC on 26 December to 19:00 UTC on 27 December 2010.

Animation 2.7c: A regional waves map animation in Lagrangian framework from 14:08 UTC on 26 December to 18:15 UTC on 27 December 2010.

Animation 3.4a: A regional reflectivity map animation from 12 February 2006 from 11:05 to 11:40 UTC (top left). A regional stitched waves animation from 12 February 2006 from

11:05 to 11:40 UTC (top right). A vertical reflectivity cross section animation from 12 February 2006 from 11:05 to 11:40 UTC (bottom right). A vertical waves cross section animation from 12 February 2006 from 11:05 to 11:40 UTC (bottom left).

Animation 3.4b: A vertical reflectivity cross section animation from 12 February 2006 from 11:05 to 11:40 UTC (top left). A vertical waves cross section animation from 12 February 2006 from 11:05 to 11:40 UTC (bottom left). A vertical radial velocity cross section animation from 12 February 2006 from 11:05 to 11:40 UTC (top right). A vertical instantaneous convergence/divergence cross section animation from 12 February 2006 from 11:05 to 11:40 UTC (bottom right).